

# Parametric Amplification of an Optomechanical Quantum Interconnect

Huo Chen,<sup>1,\*</sup> Marti Vives,<sup>2,†</sup> and Mekena Metcalf<sup>1,‡</sup>

<sup>1</sup>*Applied Mathematics and Computational Research Division,*

*Lawrence Berkeley National Laboratory, Berkeley, CA 94720, USA*

<sup>2</sup>*Department of Electrical and Computer Engineering, Princeton University, Princeton, NJ 08544, USA*

Connecting microwave quantum computing technologies with optical fiber necessitates the conversion of microwave photons to optical photons mediated by strong coupling between microwave and optical fields. Modern experimental demonstrations exhibit strong coupling between a microwave resonator and an optical cavity mediated through phononic modes in a mechanical oscillator. This paradigmatic transduction experiment is bounded by a theoretical efficiency with constant driving amplitudes on the electromagnetic resonators. By adding a parametric drive to the microwave resonator and optical cavity we can amplify the converted signal through the quantum transducer, while maintaining a lower level of the added noise. We present a theoretical framework for time-dependent control of the driving lasers based on the input-output formalism of quantum optics, and solve analytically the transduction efficiency and added noise when the control signals parametrically drive the system. Our results show better transduction efficiency and lower added noise in varying parameter regimes relevant to current transduction experiments.

**Introduction** - Coupling of photons in cavities to mechanical membranes via a radiation pressure force has developed in a rich field with wide-ranging applications [1], including high-precision measurement [2, 3], gravitational wave detection [4], nonlinear optics [5, 6], optomechanical cooling [7, 8] and nonreciprocal devices [9, 10]. In addition, it has the potential to serve as a coherent light-matter interface and interconnect otherwise incompatible degrees of freedoms within a quantum network [11–14]. Conversion of quantum information across disparate energy scales requires the development of quantum transduction technology [15]. The scaling of quantum processor technology to enable logical quantum information processing is met with limitations that depend on the underlying device physics [16–18], thus, a hybrid quantum architecture may illuminate a viable path to scalable quantum computers.

An optomechanical transducer is composed of a microwave resonator and an optical cavity each coupled to the same mechanical resonator. Experimental demonstrations validate the promise of quantum transduction, yet further progress is needed to achieve unity efficiency [13, 19]. Evolution of the electromagnetic (EM) field operators is solved using the input-output formalism of quantum optics and a linearized optomechanical Hamiltonian, yielding an analytic expression for transduction efficiency [1, 20, 21]. The analytic evaluation of the equation of motion is rendered trivial with constant driving amplitudes on the EM resonators, however, analytic bounds on efficiency with time-dependent drive signals are only accessible in special cases. We consider the special case of parametric driving of the EM cavities. Parametric driving is shown to enhance the entanglement between the cavity photon mode and the mechanical phonon mode [22]. We discovered this same driving scheme leads to an amplification of optomechanical transduction efficiency while maintaining a lower level of added noise. The low added noise is achieved through the

suppression of the two-mode-squeezing interaction (TMSI), similar to Ref. [23]. Our method differs from the reference as the noise suppression is intrinsic without the need of squeezing the noise ports. A recently study also reports similar effect of transduction efficiency enhancement [24].

In this paper, we provide an analytic solution for the parametrically driven optomechanical transducer transfer function and derive an expression for the transduction efficiency and added noise. Our results are supported by numerically evaluating amplification in existing experimental implementations. These results readily provide improvement over constant cavity driving and complement existing protocols to improve transduction performance [13, 25].

**Time-Dependent Optomechanics** - We start by formulating the Hamiltonian of the optomechanical transducer, illustrated in Fig 1. As shown in the schematic, two strong pump tones detuned from the cavity frequencies are applied to each electromagnetic (EM) resonator. We assume each of the pump tones has a time-dependent amplitude  $\Omega_i(t)$  which serves as a control signal. The Hamiltonian (in the laser frame of the pump tones) is

$$\hat{H}(t) = w_m \hat{a}_m^\dagger \hat{a}_m + \sum_i \Delta_i \hat{a}_i^\dagger \hat{a}_i + g_i \hat{x}_m \hat{a}_i^\dagger \hat{a}_i + \Omega_i(t) \hat{x}_i \quad (1)$$

where  $\hat{a}_i, \hat{a}_i^\dagger$  ( $i \in \{o, e, m\}$ ) are the bosonic annihilation and creation operators, and  $\hat{x}_i = \hat{a}_i^\dagger + \hat{a}_i$ . We also set  $\hbar = 1$ . The subscript o (optical) and e (electrical) stand for the EM modes at optical and microwave frequencies while m (mechanical) stands for the vibrational mode.  $\Delta_i = \omega_i - \omega_{il}$  is the cavity ( $\omega_i$ ) detuning with respect to the laser frequencies ( $\omega_{il}$ ), and  $g_o$  and  $g_e$  are the optomechanical single-photon coupling strength between each EM resonator and the mechanical resonator.

We derive an effective linearized Hamiltonian with time-dependent controls using the approach in [7]. The EM resonators are treated independently because the pump lasers are strong enough to dominate the resonator dynamics as  $|\Omega_i(t)| \gg \Delta_i, g_i$ . The Heisenberg equation of motion of

\* [huochen@lbl.gov](mailto:huochen@lbl.gov)

† [mvives1122@gmail.com](mailto:mvives1122@gmail.com)

‡ [mekena.metcalf@gmail.com](mailto:mekena.metcalf@gmail.com)

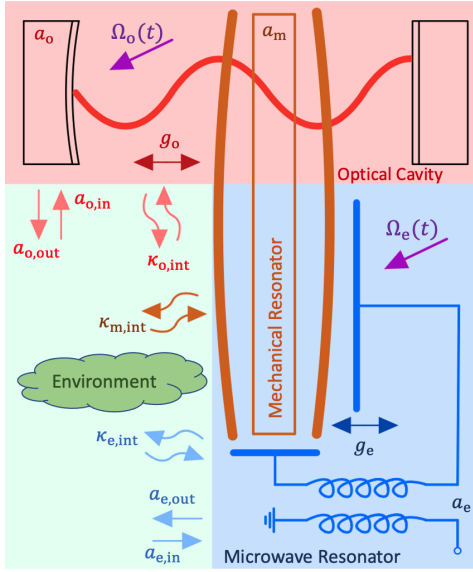


Figure 1. Schematic of an optomechanical quantum transducer. In this setup, an optical cavity and a microwave resonator couple to the same mechanical membrane, with single-photon coupling strengths  $g_o$  and  $g_e$ . Each mode also couples to their corresponding external inputs and outputs ( $\hat{a}_{i,\text{in}}$ ,  $\hat{a}_{i,\text{out}}$ ) which suffers from the internal loss ( $\kappa_{i,\text{int}}$ ). The control signals ( $\Omega_i(t)$ ) are applied to both of the electromagnetic (EM) modes via the pump lasers.

field operator  $\hat{a}_i$  for a single cavity with loss is given by

$$\dot{\alpha}_i(t) = -i\Delta_i\alpha_i(t) - \frac{\kappa_i}{2}\alpha_i(t) - i\Omega_i(t), \quad (2)$$

where  $\kappa_i$  is the energy decay rate of the cavity, and  $\alpha_i(t) = \langle \hat{a}_i(t) \rangle$  average operator value. Next we apply the perturbation technique by moving to the rotating frame of displacement operators  $\otimes_i \exp(\alpha_i(t)\hat{a}_i^\dagger - \alpha_i^*(t)\hat{a}_i)$ , and linearize the Hamiltonian ([26] Sec. A). The resulting Hamiltonian is given by

$$\hat{H}_{\text{lin}} = \omega_m \hat{a}_m^\dagger \hat{a}_m + \sum_{i=e,o} \Delta_i \hat{a}_i^\dagger \hat{a}_i + g_i |\alpha_i(t)|^2 \hat{x}_m \quad (3a)$$

$$+ (G_i^*(t)\hat{a}_i + G_i(t)\hat{a}_i^\dagger)\hat{x}_m, \quad (3b)$$

where  $G_i(t) = g_i\alpha_i(t)$ . The new  $\hat{a}_i$  and  $\hat{a}_i^\dagger$  operators in the displacement frame act as fluctuations around the average photon number  $\alpha_i(t)$ . We note that the couplings in Eq. (3b) have both the beam splitter interaction and the TMSI. The latter sets the fundamental limit for the added noise in the optomechanical quantum transducer.

The linearized Hamiltonian with a time-dependent interaction is used to model transduction of flying photons. Incoming and outgoing photons from the EM resonators are modeled as input and output ports using the input-output formalism of quantum optics [27]. The quantum Langevin equation for the Hamiltonian Eq. (3) is a time-varying linear system (see [26]

Sec. C and D for derivation) given by

$$\dot{\hat{a}}_i = -i\Delta_i\hat{a}_i - \frac{\kappa_i}{2}\hat{a}_i - iG_i\hat{x}_m + \sqrt{\kappa_{\text{ex},i}}\hat{a}_{i,\text{in}} \quad (4a)$$

$$\dot{\hat{a}}_m = -(i\omega_m + \frac{\kappa_m}{2})\hat{a}_m - i \sum_i \left( G_i^* \hat{a}_k + G_i \hat{a}_k^\dagger + |G_i|^2 \right) + \sqrt{\kappa_{\text{ex},m}}\hat{a}_{m,\text{in}}, \quad (4b)$$

where  $i \in [o, e]$ , and we omitted the time dependence of the variables.  $\kappa_{i,\text{ex}}$  is the coupling strength of mode  $i$  to the external input-output fields. If we define a state vector as  $\mathbf{a}(t) = [\hat{a}_o(t), \hat{a}_e(t), \hat{a}_o^\dagger(t), \hat{a}_e^\dagger(t), \hat{a}_m(t), \hat{a}_m^\dagger(t)]^T$ , we can write Eqs. (4) in a matrix form

$$\dot{\mathbf{a}}(t) = \mathbf{A}(t)\mathbf{a}(t) + \mathbf{B}\mathbf{a}_{\text{in}}(t) + \mathbf{v}(t), \quad (5)$$

where explicit forms of operators are given in [26] Sec. D. The input and output are connected via the following relation [27] (see also [26], Sec. C and D)

$$\mathbf{a}_{\text{out}}(t) + \mathbf{a}_{\text{in}}(t) = \mathbf{B}\mathbf{a}(t). \quad (6)$$

For Eq. (5) and Eq. (6) to share the same  $\mathbf{B}$  matrix, we assume each resonator is connected to only one pair of external input and output. All the other inputs and outputs (i.e., internal loss) are omitted because they become 0 if we average Eq. (5) over the initial state. We call those omitted terms the implicit inputs and outputs and discuss their roles in the added noise of quantum transduction in a later section.

The goal of this quantum transducer is to convert one photon from the input of the electrical resonator to the output of the optical resonator, or vice versa.

**Parametrically Driven System -** When the control signals are constant,  $\Omega_i(t) = \Omega_i$ , previous studies have shown that the maximum efficiency is achieved when the input state frequency matches the mechanical frequency  $\omega_m$  (in the laser frame)[19]. We can improve this transduction efficiency via parametric amplification [22, 28] by choosing oscillating control signals at twice the input signal frequency  $\Omega_i(t) = \Omega_i e^{-2i\omega_m t}$  (also referred to as parametric drive (PD) in this paper). We provide the main results and a detailed derivation is found in [26] Sec. E.

In the long time limit, the steady state of Eq. (2) subject to the oscillating control is given by

$$\alpha_i(t) = \frac{2\Omega_i}{4\omega_m - 2\Delta_i + i\kappa_i} e^{-2i\omega_m t}. \quad (7)$$

It has only a single-frequency component. As a result, the steady state  $A(t)$  matrix can be decomposed into a Fourier series

$$\mathbf{A}(t) = \mathbf{A}_d + \mathbf{A}_- e^{-2i\omega_m t} + \mathbf{A}_+ e^{2i\omega_m t}, \quad (8)$$

where  $\mathbf{A}_d$ ,  $\mathbf{A}_-$  and  $\mathbf{A}_+$  are constant matrices.  $\mathbf{A}_d$  is a diagonal matrix constructed from the diagonal elements of  $\mathbf{A}(t)$ .  $\mathbf{A}_-$  and  $\mathbf{A}_+$  are constructed from the off-diagonal elements of  $\mathbf{A}(t)$  (See [26] Sec. E for their explicit forms).

It is convenient to examine the equation of motion in the Fourier space with  $\mathbf{A}(t)$  given in Eq. (8). We obtain

$$-i\omega\mathbf{a}(\omega) = \mathbf{A}_d\mathbf{a}(\omega) + \mathbf{A}_-\mathbf{a}(\omega - 2\omega_m) + \mathbf{A}_+\mathbf{a}(\omega + 2\omega_m) + \mathbf{B}\mathbf{a}_{in}(\omega) + \mathbf{v}(\omega) \quad (9)$$

by taking Fourier transform on both sides of Eq. (5) [29]. We observe that the control signals introduce sidebands shifted by  $\pm 2\omega_m$ . While solving Eq. (9) is extremely difficult, we can proceed with a few approximations. First, we ignore the vector  $\mathbf{v}(\omega)$ . This is permissible because in the steady state  $\mathbf{v}(t)$  is constant and translates to a Dirac delta function centered at  $\omega = 0$  in the frequency domain. As long as  $\mathbf{v}(0)$  is not involved in our calculation, this term can be safely ignored. Second, we assume  $|G_i(t)|$  is small compared to the detunings  $\Delta_i$  and  $\omega_m$ , which is usually true in a typical experimental setup. This condition means the effective modulation of the control signals on our system is weak. Therefore, we can truncate the number of sidebands, or effectively the number of equations generated by Eq. (9). Assume we keep only the nearest  $2N$  sidebands, a new state vector can be defined as  $\bar{\mathbf{a}}(\omega) = [\mathbf{a}^T(\omega - 2N\omega_m), \dots, \mathbf{a}^T(\omega), \dots, \mathbf{a}^T(\omega + 2N\omega_m)]^T$ . Then Eq. (9) can be rewritten as

$$-i\bar{\mathbf{W}}\bar{\mathbf{a}}(\omega) = \bar{\mathbf{A}}\bar{\mathbf{a}}(\omega) + \bar{\mathbf{B}}\bar{\mathbf{a}}_{in}(\omega), \quad (10)$$

where

$$\bar{\mathbf{A}} = \begin{pmatrix} \mathbf{A}_d & \mathbf{A}_+ & 0 & \dots & 0 \\ \mathbf{A}_- & \mathbf{A}_d & \mathbf{A}_+ & & 0 \\ 0 & \mathbf{A}_- & \mathbf{A}_d & & \vdots \\ \vdots & & & \ddots & \mathbf{A}_+ \\ 0 & 0 & \dots & \mathbf{A}_- & \mathbf{A}_d \end{pmatrix}, \quad (11)$$

and  $\bar{\mathbf{B}} = \text{diag}(\mathbf{B}, \mathbf{B}, \dots, \mathbf{B})$ . The input vector  $\bar{\mathbf{a}}_{in}(\omega) = [\mathbf{a}_{in}^T(\omega - 2N\omega_m), \dots, \mathbf{a}_{in}^T(\omega), \dots, \mathbf{a}_{in}^T(\omega + 2N\omega_m)]^T$ , and  $\bar{\mathbf{W}}$  is a block diagonal matrix with the corresponding shifted frequencies in each block. Based on Eq. (10) and the Fourier transform of the input-output relation (Eq. (6)), we can solve for the output vector at the central frequency. The solution is given by (See [26] Sec. E2 for derivations)

$$\mathbf{a}_{out}(\omega) = \mathbf{T}(\omega)\mathbf{a}_{in}(\omega) + \sum_{i=1}^N \mathbf{T}_{\pm}^{[k]}(\omega)\mathbf{a}_{in}(\omega \pm 2k\omega_m). \quad (12)$$

$\mathbf{T}(\omega)$  and  $\mathbf{T}_{\pm}^{[k]}(\omega)$  are known as the transfer matrices. Eq. (12) suggests that, besides the input at the central frequency, input at other sidebands can also be mixed into the output via  $\mathbf{T}_{\pm}^{[k]}(\omega)$ . The explicit forms of the transfer matrices are given by

$$\mathbf{T}(\omega) = \mathbf{B}\mathbf{X}(\omega)\mathbf{B} - \mathbf{I} \quad (13a)$$

$$\mathbf{T}_{\pm}^{[k]}(\omega) = \mathbf{B}\mathbf{X}(\omega) \prod_{i=1}^k (\mathbf{A}_{\pm}\mathbf{X}_{\pm}^{[i]}(\omega))\mathbf{B}, \quad (13b)$$

where  $\mathbf{X}_{\pm}^{[i]}(\omega)$  can be obtained using the recursive relation

$$\mathbf{X}_{\pm}^{[k]}(\omega) = \left[ -i(\omega \pm 2k\omega_m)\mathbf{I} - \mathbf{A}_d - \mathbf{\Xi}_{\pm}^{[k+1]}(\omega) \right]^{-1} \quad (14a)$$

$$\mathbf{\Xi}_{\pm}^{[k]}(\omega) = \mathbf{A}_{\pm}\mathbf{X}_{\pm}^{[k]}(\omega)\mathbf{A}_{\mp}, \quad (14b)$$

with the boundary condition

$$\mathbf{X}_{\pm}^{[N]}(\omega) = [-i(\omega \pm 2N\omega_m)\mathbf{I} - \mathbf{A}_d]^{-1}. \quad (15)$$

In addition, the matrix  $\mathbf{X}(\omega)$  is

$$\mathbf{X}(\omega) = \left( -i\omega\mathbf{I} - \mathbf{A}_d - \mathbf{\Xi}_{-}^{[1]}(\omega) - \mathbf{\Xi}_{+}^{[1]}(\omega) \right)^{-1}. \quad (16)$$

The symbol  $\mathbf{I}$  represents the identity matrix of the same dimension as  $\mathbf{A}(t)$ .

Given the general form of Eq. (12), we present the main results of this paper (see [26] Sec. G for the proof). The first result states that  $\mathbf{T}(\omega)$  has a block diagonal structure

$$\mathbf{T}(\omega) = \begin{pmatrix} \mathbf{T}_a(\omega) & 0 & 0 \\ 0 & \mathbf{T}_c(\omega) & 0 \\ 0 & 0 & \mathbf{T}_m(\omega) \end{pmatrix}, \quad (17)$$

where  $\mathbf{T}_i(\omega)$ s are  $2 \times 2$  matrices. There are three immediate consequences of Eq. (17). The first consequence is that there are no conjugate transmissions in  $\mathbf{T}(\omega)$ , i.e.,  $\mathbf{T}_{i,j}(\omega) = 0$  for any  $i$  and  $j$ , where  $\mathbf{T}_{i,j}(\omega)$  is a shorthand notation for

$$\mathbf{T}_{i,j}(\omega) = \frac{\hat{a}_{i,out}(\omega)}{\hat{a}_{j,in}(\omega)}, \quad \mathbf{T}_{i,j}(\omega) = \frac{\hat{a}_{i,out}(\omega)}{\hat{a}_{j,in}(\omega)}. \quad (18)$$

This statement implies that our protocol suppresses the TMSI, thus effectively reducing the added noise in the output signal. The second consequence is that the mechanical input at the central frequency is decoupled from the EM outputs, which indicates the parametrically driven transducer has built-in tolerance for mechanical noise at the central frequency. The last consequence is that any energy coming from the mechanical inputs at the central frequency will be trapped within the mechanical mode, thus enhancing the excitation of mechanical phonons. Such enhancement can lead to amplification of the transduction efficiency, provided that the system is stable.

The second result states that  $\mathbf{T}_{\pm}^{[k]}(\omega) = 0$  for  $k > 2$ . Furthermore, by examining the structure of  $\mathbf{T}_{\pm}^{[1]}(\omega)$

$$\mathbf{T}_{+}^{[1]} = \begin{pmatrix} 0 & 0 & 0 \\ 0 & 0 & \mathbf{T}_{cm} \\ \mathbf{T}_{ma} & 0 & 0 \end{pmatrix}, \quad \mathbf{T}_{-}^{[1]} = \begin{pmatrix} 0 & 0 & \mathbf{T}_{am} \\ 0 & 0 & 0 \\ 0 & \mathbf{T}_{mc} & 0 \end{pmatrix}, \quad (19)$$

and  $\mathbf{T}_{\pm}^{[2]}(\omega)$

$$\mathbf{T}_{+}^{[2]} = \begin{pmatrix} 0 & 0 & 0 \\ \mathbf{T}_{ca} & 0 & 0 \\ 0 & 0 & 0 \end{pmatrix}, \quad \mathbf{T}_{-}^{[2]} = \begin{pmatrix} 0 & \mathbf{T}_{ac} & 0 \\ 0 & 0 & 0 \\ 0 & 0 & 0 \end{pmatrix}, \quad (20)$$

we discover  $\mathbf{T}_{\pm}^{[1]}(\omega)$  only couples the EM outputs to the mechanical input of the nearest sidebands, while  $\mathbf{T}_{\pm}^{[2]}(\omega)$  only

couples the EM outputs to the conjugate components of the EM inputs. For example, if we consider the output of the optical cavity, the only terms being mixed into  $\hat{a}_{o,out}(\omega)$  by  $\mathbf{T}_{\pm}^{[k]}(\omega)$  are

$$\begin{aligned}\hat{a}_{o,out}(\omega) &= \dots \\ &+ \mathbf{U}_{o,m}\hat{a}_{m,in}(\omega - 2\omega_m) + \mathbf{U}_{o,m^\dagger}\hat{a}_{m,in}^\dagger(\omega - 2\omega_m) \quad (21a) \\ &+ \mathbf{V}_{o,e^\dagger}\hat{a}_{e,in}(\omega - 4\omega_m) + \mathbf{V}_{o,o^\dagger}\hat{a}_{o,in}^\dagger(\omega - 4\omega_m), \quad (21b)\end{aligned}$$

where  $\mathbf{U} = \mathbf{T}_{-}^{[1]}(\omega)$  and  $\mathbf{V} = \mathbf{T}_{+}^{[2]}(\omega)$ . In Eq. (19) and (20),  $\mathbf{T}_{ij}$ s are  $2 \times 2$  matrices and we omitted the frequency dependence. Eq. (21) indicates that our strategy trades the central frequency mechanical noise with the sideband frequency noise. It will become beneficial when the mechanical mode has negligible coupling to inputs at the sideband frequencies  $2\omega_m \gg \kappa_m$ .

**Ideal Transducer -** In this section, we apply the general theory to an ideal quantum transducer. We assume the pump lasers are perfectly red detuned from the corresponding cavity frequencies by  $\omega_m$ , i.e.,  $\Delta_o = \Delta_e = \omega_m$ . We also assume the electrical and optical cavities are symmetric and have no internal loss, i.e.,  $\kappa_{e,ex} = \kappa_{o,ex} = \kappa_e = \kappa_o = \kappa$ ,  $g_e = g_o$ , and  $\Omega_o = \Omega_e$ . We consider the scenario where all the inputs are in the vacuum or thermal state except for the one connected to the electrical cavity, which is in the single-frequency coherent state with an average of one photon. The goal of this experiment is to convert the input microwave photon to an output optical photon. The relevant figure of merits are the transduction efficiency and the added noise, both defined in the frequency domain. The former is defined as  $\eta(\omega) \equiv |\mathbf{T}_{o,e}(\omega)|$ , and the latter is defined as [23, 30]

$$2\pi\eta^2(\omega)S(\omega)\delta(\omega - \omega') = \frac{1}{2} \left\langle \left\{ \hat{J}(\omega), \hat{J}(\omega')^\dagger \right\} \right\rangle, \quad (22)$$

where  $\hat{J}(\omega)$  is the noise terms being mixed into the output. We emphasize here that  $S(\omega)$  is obtained from the second order moments, thus contains more terms than explicitly defined in the equation of motion Eq. (5). We split  $\hat{J}(\omega)$  into explicit and implicit parts  $\hat{J}(\omega) = \hat{J}_{ex}(\omega) + \hat{J}_{im}(\omega)$  where

$$\begin{aligned}\hat{J}_{ex}(\omega) &= \mathbf{T}_{o,e^\dagger}(\omega)\hat{a}_{e,in}^\dagger(\omega) \\ &+ \mathbf{T}_{o,o}(\omega)\hat{a}_{o,in}(\omega) + \mathbf{T}_{o,o^\dagger}(\omega)\hat{a}_{o,in}^\dagger(\omega), \quad (23)\end{aligned}$$

and  $\hat{J}_{im}(\omega)$  contains all the implicitly defined inputs, e.g., the internal loss and inputs at sideband frequencies (Eq. (21)). Without loss of generality, we assume it has the form of  $\hat{J}_{im}(\omega) = \sum_i \mathbf{T}_{o,i}(\omega)\hat{a}_{i,in} + \mathbf{T}_{o,i^\dagger}(\omega)\hat{a}_{i,in}^\dagger$ . Then the added noise can be calculated directly from the elements of the transfer matrices

$$S(\omega) = \frac{3}{2}R^2(\omega) + \sum_k \left[ \frac{|\mathbf{T}_{o,k}(\omega)|^2}{2\eta^2(\omega)} + \frac{|\mathbf{T}_{o,k^\dagger}(\omega)|^2}{2\eta^2(\omega)} \right], \quad (24)$$

where  $R^2(\omega) = |\mathbf{T}_{o,e^\dagger}(\omega)|^2/\eta^2(\omega)$ , and the unwanted (conjugate) reflection in Eq. (23) are included in the summands. A

lower bound for  $S(\omega)$  resulting the preservation of commutation relation is derived [23] (see [26] Sec. F)

$$S(\omega) \geq \frac{3}{2}R^2(\omega) + \left| \frac{1 - \eta^2(\omega)}{2\eta^2(\omega)} + \frac{R^2(\omega)}{2} \right|. \quad (25)$$

This lower bound contains only the transduction efficiency  $\eta(\omega)$  and the conjugate transmission coefficient  $\mathbf{T}_{o,e^\dagger}(\omega)$ , even though there are other inputs being coupled to the output. It states that there will be excessive noise if the transduction efficiency goes beyond unity. Because the input signal frequency is  $\omega_m$ , we will focus on  $\eta(\omega_m)$  and  $S(\omega_m)$ .

First we consider the limit of zero mechanical loss  $\kappa_m \rightarrow 0$ . If we keep only the nearest two sidebands in Eq. (15), i.e.,  $N = 1$ , the  $\mathbf{T}(\omega)$  elements become (See [26] Sec. E 2 and [31])

$$\eta(\omega_m) \equiv |\mathbf{T}_{o,e}(\omega_m)| = 1 \quad (26a)$$

$$\mathbf{T}_{o,e^\dagger}(\omega_m) = \mathbf{T}_{o,o^\dagger}(\omega_m) = \mathbf{T}_{o^\dagger,o^\dagger}(\omega_m) = 0. \quad (26b)$$

Eqs. (26) indicate that weak oscillating control can suppress all the unwanted noise, including TMSI, in an ideal symmetric quantum transducer. This leads to high-fidelity transduction even if the transducer is in the sideband unresolved limit  $4\omega_m \lesssim \kappa$ . In this regard, our protocol is similar to the one proposed in [23], with an extra benefit of not requiring any additional squeezing of the inputs.

We emphasize that the suppression of conjugate transmission and reflection ( $\mathbf{T}_{o,e^\dagger}$  and  $\mathbf{T}_{o,o^\dagger}$  respectively) is due to the block-diagonal structure of  $\mathbf{T}$  (see Eq. (17)), thus is true for any choice of  $N$ . If we consider the case of  $N = 2$

$$\mathbf{T}_{o,e}(\omega_m) = -1 + \frac{i\kappa}{4\omega_m}, \quad \mathbf{T}_{o,o}(\omega_m) = \frac{i\kappa}{4\omega_m}, \quad (27)$$

we notice that additional noise is introduced by the reflection ( $\mathbf{T}_{o,o}$ ) and coupling to the lower sideband input  $|\mathbf{V}_{o,e}| = |\mathbf{V}_{o,e^\dagger}| = \kappa/4\omega_m$ . These noises can be suppressed by deliberately impedance mismatching the system while squeezing the optical output and electrical input at the lower sideband frequency  $\omega - 4\omega_m$  [23]. However, as demonstrated in Fig 2, even if no further action is taken, the PD protocol introduces less noise than the constant one.

Next, we show that for a transducer with non-vanishing  $\kappa_m$ , the PD strategy enhances transduction efficiency with less added noise when  $\kappa_m$  is small. Such enhancement is caused by the additional energy being trapped inside the mechanical mode. The main result is illustrated in Fig 2, where we plot the transduction efficiency and added noise of a symmetric quantum transducer with different  $\kappa_m$  values. The parameters are adapted from a real-world experiment [13], and we consider the solution of the constant control, and the oscillating control with  $N = 1$  and  $N = 2$ . In the lower panel of Fig 2, we plot the both  $S(\omega_m)$  and its lower bound (Eq. (24) and (25)) for these three solutions. We observe that more noise is introduced to the output when  $\kappa_m$  increases. However, when the noise is below the classical limit, the PD solutions always have less added noise than the constant one. These regions are also denoted in the upper panel of Fig 2 by

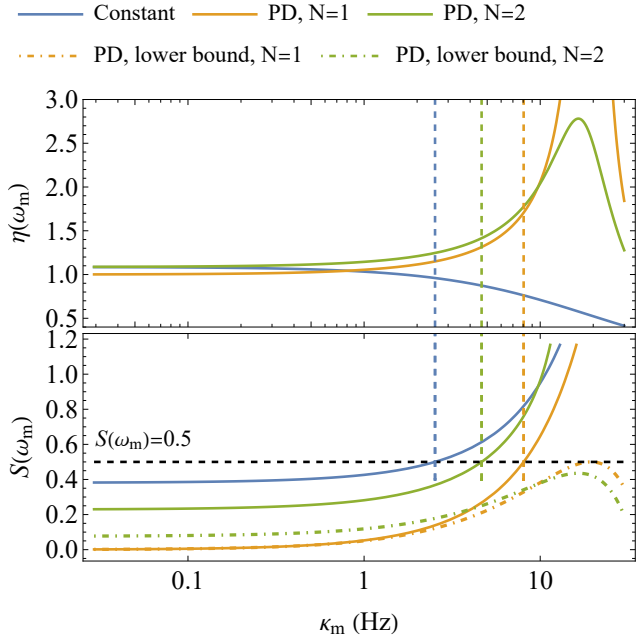


Figure 2. Transduction efficiency  $\eta(\omega_m)$  and added noise  $S(\omega_m)$  of a symmetric optomechanical transducer with different mechanical decay rate  $\kappa_m$ . The solid lines represent the solutions with constant or parametric drive (PD).  $2N$  denotes the number of sidebands being kept in Eq. (10). Upper panel: the dashed lines denote the  $\kappa_m$  values where the added noise reach the classical limit  $S(\omega_m) = 0.5$  for the corresponding solutions. Lower panel: the dash-dotted lines are the lower bounds of  $S(\omega_m)$  given by Eq. (25); the black dashed line denote the classical limit of added noise  $S(\omega_m) = 0.5$ . The parameters used in the calculation are symmetric for both the radio frequency cavities, meaning  $\kappa_{e,\text{ex}} = \kappa_{o,\text{ex}} = \kappa_e = \kappa_o = \kappa$ ,  $g_e = g_o = g$ , and  $\Omega_o = \Omega_e = \Omega$ . Their numerical values are:  $\omega_m/2\pi = 1.4732$  MHz,  $\kappa/2\pi = 2.5$  MHz,  $g/2\pi = 3.8$  Hz and  $\Omega/2\pi = 500$  MHz. In addition, the mechanical oscillator has a single input-output port  $\kappa_{m,\text{ex}} = \kappa_m$ .

dashed lines. Within the regions of acceptable noise, larger  $\kappa_m$  leads to higher transduction efficiency of the PD solutions but lower efficiency of the constant solution. Consequently the transduction efficiency is amplified by PD from approximately  $\kappa_m \gtrsim 1$  (Hz). In practice, we can fine tune the efficiency to unity by impedance mismatching the system to further reduce the noise level.

**Realistic Transducer -** In the ideal case, because the efficiency is already closed to unity, the main benefit of the PD strategy is to reduce the added noise. However, this strategy is equally useful on a realistic optomechanical quantum transducer [13], where perfect impedance match is hard to achieve due to experimental constraints, thus limiting the transduction efficiency. In this section we demonstrate that the PD protocol offers better transduction efficiency while maintaining a lower added noise level than the constant control for some parameter regimes. Our analysis is based on the experimental configuration presented in [13]. Unfortunately, the experiment works in a noisy regime, i.e.,  $S(\omega_m) > 0.5$ , and the authors adopted a classical feed-forward protocol to reduce the added noise.

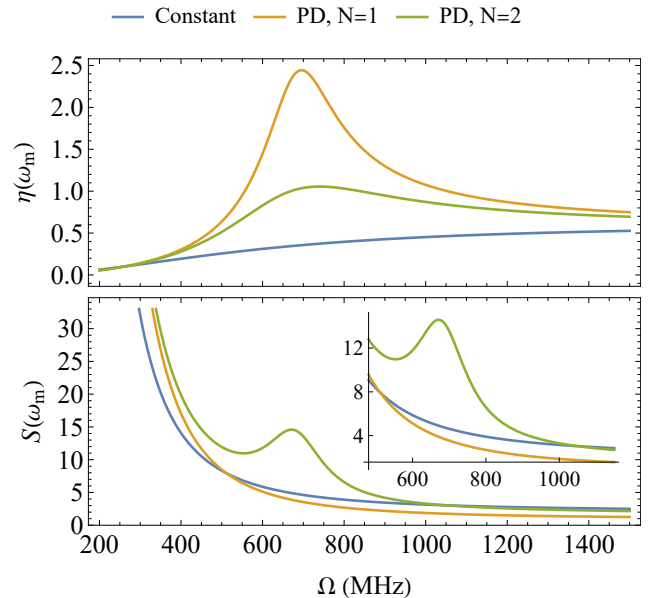


Figure 3. Transduction efficiency  $\eta(\omega_m)$  and added noise  $S(\omega_m)$  of a realistic optomechanical quantum transducer [13] with different driving amplitude  $\Omega_o = \Omega_e = \Omega$ . The solid lines represent the solutions with constant or parametric drive (PD).  $2N$  denotes the number of sidebands being kept in Eq. (10). The inset in the lower panel shows a zoomed-in version of the same plot. The numerical values used in the calculation are given in Table I of [26].

While it is not clear whether a quantum feed-forward protocol exists to further reduce  $S(\omega_m)$ , we still choose to work in the same parameter regime because our main goal is to show that PD strategy can readily improve the performance of an existing experimental transducer.

In addition to the inputs defined in Eq. (4), we include in our analysis the internal loss of both the EM resonators. We also assume all the noise inputs are in the vacuum state. All the parameter values can be found in [26] Sec. H. Our results are reported in Fig 3. In the upper panel we report the transduction efficiency, and show it can be tuned by adjusting the driving signal amplitude  $\Omega_i$ , which are chosen to be the same for both the EM resonators. The PD offers higher transduction efficiency than constant drive starting from  $\Omega \gtrsim 270$  (MHz). In the lower panel we report the add noise for the same range of  $\Omega$  values. Our results show that when  $\Omega \gtrsim 512$  (MHz), the PD  $N = 1$  solution has lower noise level than the constant drive. For the PD  $N = 2$  solution, the advantage start from  $\Omega \gtrsim 1052$  (MHz) and is smaller than the previous case. Finally, we emphasize that the added noise is obtained by assuming all the noise inputs are in the vacuum state. In practice, the mechanical mode suffers from the optical-absorption-induced thermal noise [32, 33]. Thus we expect the constant drive to suffer much higher  $S(\omega_m)$  than the PD because PD decouples the mechanical inputs at the central frequency to the outputs. However, a detailed noise model needs to be developed before we can further analyze the effects of the optical-absorption-induced thermal bath.

**Conclusion and outlook -** In this paper we present a the-

oretical analysis of the optomechanical quantum transducer with time-dependent controls. We demonstrate that, without introducing more noise, better transduction efficiency can be achieved by replacing constant controls with oscillating ones. The improvement is applicable to existing experimental architectures. We hope this new development paves the way for more advanced time-dependent control protocols which, judging by the great success they have brought in designing quantum gates [34–36], may lead to even better transducer

performance.

**Acknowledgments** - The authors are grateful to Jie Luo, Zhi (Jackie) Yao, John Bell, Anastasiia Butko, Mariam Kiran and Wibe A. de Jong for useful discussions and feedback. This work was supported by the Laboratory Directed Research and Development Program of Lawrence Berkeley National Laboratory under U.S. Department of Energy Contract No. DE-AC02-05CH11231.

---

[1] M. Aspelmeyer, T. J. Kippenberg, and F. Marquardt, *Reviews of Modern Physics* **86**, 1391 (2014).

[2] A. A. Clerk, M. H. Devoret, S. M. Girvin, F. Marquardt, and R. J. Schoelkopf, *Rev. Mod. Phys.* **82**, 1155 (2010).

[3] M. S. Hanay, S. I. Kelber, C. D. O’Connell, P. Mulvaney, J. E. Sader, and M. L. Roukes, *Nat. Nanotechnol.* **10**, 339 (2015).

[4] L. Collaboration and V. Collaboration, *Physical Review Letters* **116**, 061102 (2016).

[5] J. T. Hill, A. H. Safavi-Naeini, J. Chan, and O. Painter, *Nat. Commun.* **3**, 1196 (2012).

[6] A. H. Safavi-Naeini, S. Gröblacher, J. T. Hill, J. Chan, M. Aspelmeyer, and O. Painter, *Nature* **500**, 185 (2013).

[7] S. Machnes, J. Cerrillo, M. Aspelmeyer, W. Wieczorek, M. B. Plenio, and A. Retzker, *Physical Review Letters* **108**, 153601 (2012).

[8] M. Rossi, D. Mason, J. Chen, Y. Tsaturyan, and A. Schliesser, *Nature* **563**, 53 (2018).

[9] G. A. Peterson, F. Lecocq, K. Cicak, R. W. Simmonds, J. Aumentado, and J. D. Teufel, *Phys. Rev. X* **7**, 031001 (2017).

[10] N. R. Bernier, L. D. Tóth, A. Koottandavida, M. A. Ioannou, D. Malz, A. Nunnenkamp, A. K. Feofanov, and T. J. Kippenberg, *Nat. Commun.* **8**, 604 (2017).

[11] D. Awschalom, K. K. Berggren, H. Bernien, S. Bhade, L. D. Carr, P. Davids, S. E. Economou, D. Englund, A. Faraon, M. Fejer, S. Guha, M. V. Gustafsson, E. Hu, L. Jiang, J. Kim, B. Korzh, P. Kumar, P. G. Kwiat, M. Lončar, M. D. Lukin, D. A. Miller, C. Monroe, S. W. Nam, P. Narang, J. S. Orcutt, M. G. Raymer, A. H. Safavi-Naeini, M. Spiropulu, K. Srinivasan, S. Sun, J. Vučković, E. Waks, R. Walsworth, A. M. Weiner, and Z. Zhang, *PRX Quantum* **2**, 017002 (2021).

[12] J. I. Cirac, P. Zoller, H. J. Kimble, and H. Mabuchi, *Physical Review Letters* **78**, 3221 (1997).

[13] A. P. Higginbotham, P. Burns, M. Urmey, R. Peterson, N. Kampe, B. Brubaker, G. Smith, K. Lehnert, and C. Regal, *Nature Physics* **14**, 1038 (2018).

[14] M. Mirhosseini, A. Sipahigil, M. Kalaei, and O. Painter, *Nature* **588**, 599 (2020).

[15] N. Lauk, N. Sinclair, S. Barzanjeh, J. P. Covey, M. Saffman, M. Spiropulu, and C. Simon, *Quantum Sci. Technol.* **5**, 020501 (2020).

[16] F. Arute, K. Arya, R. Babbush, D. Bacon, J. C. Bardin, R. Barends, R. Biswas, S. Boixo, F. G. S. L. Brandao, D. A. Buell, B. Burkett, Y. Chen, Z. Chen, B. Chiaro, R. Collins, W. Courtney, A. Dunsworth, E. Farhi, B. Foxen, A. Fowler, C. Gidney, M. Giustina, R. Graff, K. Guerin, S. Habegger, M. P. Harrigan, M. J. Hartmann, A. Ho, M. Hoffmann, T. Huang, T. S. Humble, S. V. Isakov, E. Jeffrey, Z. Jiang, D. Kafri, K. Kechedzhi, J. Kelly, P. V. Klimov, S. Knysh, A. Korotkov, F. Kostritsa, D. Landhuis, M. Lindmark, E. Lucero, D. Lyakh, S. Mandrà, J. R. McClean, M. McEwen, A. Megrant, X. Mi, K. Michelsen, M. Mohseni, J. Mutus, O. Naaman, M. Neeley, C. Neill, M. Y. Niu, E. Ostby, A. Petukhov, J. C. Platt, C. Quintana, E. G. Rieffel, P. Roushan, N. C. Rubin, D. Sank, K. J. Satzinger, V. Smelyanskiy, K. J. Sung, M. D. Trevithick, A. Vainsencher, B. Villalonga, T. White, Z. J. Yao, P. Yeh, A. Zalcman, H. Neven, and J. M. Martinis, *Nature* **574**, 505 (2019).

[17] H.-S. Zhong, H. Wang, Y.-H. Deng, M.-C. Chen, L.-C. Peng, Y.-H. Luo, J. Qin, D. Wu, X. Ding, Y. Hu, P. Hu, X.-Y. Yang, W.-J. Zhang, H. Li, Y. Li, X. Jiang, L. Gan, G. Yang, L. You, Z. Wang, L. Li, N.-L. Liu, C.-Y. Lu, and J.-W. Pan, *Science* **370**, 1460 (2020).

[18] C. Figgatt, A. Ostrander, N. M. Linke, K. A. Landsman, D. Zhu, D. Maslov, and C. Monroe, *Nature* **572**, 368 (2019).

[19] R. W. Andrews, R. W. Peterson, T. P. Purdy, K. Cicak, R. W. Simmonds, C. A. Regal, and K. W. Lehnert, *Nature physics* **10**, 321 (2014).

[20] F. Lecocq, J. B. Clark, J. A. R. W. Simmonds, and J. D. Teufel, *Physical Review Letters* **116**, 043601 (2016).

[21] L. Tian and H. Wang, *Physical Review A* **82**, 053806 (2010).

[22] A. Mari and J. Eisert, *Phys. Rev. Lett.* **103**, 213603 (2009).

[23] H.-K. Lau and A. A. Clerk, *Phys. Rev. Lett.* **124**, 103602 (2020).

[24] C. Zhong, M. Xu, A. Clerk, H. X. Tang, and L. Jiang, *Quantum transduction is enhanced by single mode squeezing operators* (2022), [arXiv:2204.05521 \[quant-ph\]](https://arxiv.org/abs/2204.05521).

[25] M. Zhang, C.-L. Zou, and L. Jiang, *Phys. Rev. Lett.* **120**, 020502 (2018).

[26] See Supplemental Material for additional details.

[27] C. W. Gardiner and M. J. Collett, *Phys. Rev. A Gen. Phys.* **31**, 3761 (1985).

[28] A. A. Clerk, M. H. Devoret, S. M. Girvin, F. Marquardt, and R. J. Schoelkopf, *Rev. Mod. Phys.* **82**, 1155 (2010).

[29] We use  $\int f(t)e^{i\omega t} dt$  as the Fourier transform convention.

[30] C. M. Caves, *Phys. Rev. D* **26**, 1817 (1982).

[31] A companion mathematica notebook can be found in this github repo: [https://github.com/neversakura/parametric\\_amplified\\_transducer](https://github.com/neversakura/parametric_amplified_transducer).

[32] H. Ren, M. H. Matheny, G. S. MacCabe, J. Luo, H. Pfeifer, M. Mirhosseini, and O. Painter, *Nat. Commun.* **11**, 3373 (2020).

[33] G. S. MacCabe, H. Ren, J. Luo, J. D. Cohen, H. Zhou, A. Sipahigil, M. Mirhosseini, and O. Painter, *Science* **370**, 840 (2020).

[34] M. Y. Niu, S. Boixo, V. N. Smelyanskiy, and H. Neven, *npj Quantum Information* **5**, 1 (2019).

[35] M. Werninghaus, D. J. Egger, F. Roy, S. Machnes, F. K. Wilhelm, and S. Filipp, *npj Quantum Information* **7**, 1 (2021).

[36] Y. Baum, M. Amico, S. Howell, M. Hush, M. Liuzzi, P. Mundada, T. Merkh, A. R. R. Carvalho, and M. J. Biercuk, [arXiv:2105.01079 \[cond-mat, physics:quant-ph\]](https://arxiv.org/abs/2105.01079) (2021).

## Appendix A: Interaction Picture Hamiltonian

In this section, we derive the interaction picture Hamiltonian with respect to the displacement operator  $\hat{\mathcal{D}} = \otimes_i \hat{\mathcal{D}}_i(\alpha_i(t))$ . First, we know the displacement operator satisfies the following three equations:

$$\hat{\mathcal{D}}^\dagger(\alpha)\hat{a}\hat{\mathcal{D}}(\alpha) = \hat{a} + \alpha, \quad \hat{\mathcal{D}}^\dagger(\alpha)\hat{a}^\dagger\hat{\mathcal{D}}(\alpha) = \hat{a}^\dagger + \alpha^*, \quad (\text{A1})$$

$$\hat{\mathcal{D}}^\dagger(\alpha)\hat{a}^\dagger\hat{a}\hat{\mathcal{D}}(\alpha) = \hat{\mathcal{D}}^\dagger(\alpha)\hat{a}^\dagger\hat{\mathcal{D}}(\alpha)\hat{\mathcal{D}}^\dagger(\alpha)\hat{a}\hat{\mathcal{D}}(\alpha) = (\hat{a}^\dagger + \alpha^*)(\hat{a} + \alpha). \quad (\text{A2})$$

Using Eqs. (A1), we can write down the interaction picture Hamiltonian as

$$\hat{\tilde{H}} \equiv \hat{\mathcal{D}}^\dagger\hat{H}\hat{\mathcal{D}} - i\hat{\mathcal{D}}^\dagger\dot{\hat{\mathcal{D}}} = \omega_m\hat{b}^\dagger\hat{b} + \sum_{i=e,o} \Delta_i(\hat{a}_i^\dagger + \alpha_i^*)(\hat{a}_i + \alpha_i) \quad (\text{A3a})$$

$$+ g_i(\hat{a}_i^\dagger + \alpha_i^*)(\hat{a}_i + \alpha_i)\hat{x}_m + \Omega_i(\hat{a}_i^\dagger + \hat{a}_i + \alpha_i + \alpha_i^*) \quad (\text{A3b})$$

$$+ i(\dot{\alpha}_i^*\hat{a}_i - \dot{\alpha}_i\hat{a}_i^\dagger). \quad (\text{A3c})$$

The geometric terms in line (A3c) (see Appendix B for derivation) can be simplified by plugging

$$\dot{\alpha}_i(t) = -i\Delta_i\alpha_i(t) - \frac{\kappa_i}{2}\alpha_i(t) - i\Omega_i(t), \quad (\text{A4})$$

into the expression, which leads to

$$i(\dot{\alpha}_i^*\hat{a}_i - \dot{\alpha}_i\hat{a}_i^\dagger) = -\Delta_i(\alpha_i^*(t)\hat{a}_i + \alpha_i(t)\hat{a}_i^\dagger) - i\frac{\kappa_i}{2}\alpha^*(t)\hat{a}_i + i\frac{\kappa_i}{2}\alpha_i(t)\hat{a}_i^\dagger - \Omega_i(t)(\hat{a}_i + \hat{a}_i^\dagger). \quad (\text{A5})$$

We make the following two approximations. First, we ignore all terms that are proportional to identity. Second, we ignore the second order term in the interaction Hamiltonian. As a result, we have

$$g_i(\hat{a}_i^\dagger + \alpha_i^*(t))(\hat{a}_i + \alpha_i(t))\hat{x}_m \approx g_i(\alpha_i(t)\hat{a}_i^\dagger + \alpha_i^*(t)\hat{a}_i)\hat{x}_m + g_i|\alpha_i(t)|^2\hat{x}_m. \quad (\text{A6})$$

Finally the time-dependent linearized Hamiltonian is given by

$$\hat{H}_{\text{lin}} = \omega_m\hat{a}_m^\dagger\hat{a}_m + \sum_{i=e,o} \Delta_i\hat{a}_i^\dagger\hat{a}_i + (G_i^*(t)\hat{a}_i + G_i(t)\hat{a}_i^\dagger)\hat{x}_m + g_i|\alpha_i(t)|^2\hat{x}_m \quad (\text{A7a})$$

$$- i\frac{\kappa_i}{2}\alpha^*(t)\hat{a}_i + i\frac{\kappa_i}{2}\alpha_i(t)\hat{a}_i^\dagger, \quad (\text{A7b})$$

where  $G_i(t) = g_i\alpha_i(t)$ . The open system effects  $\kappa_i$  in the geometry term (line (A7b)) will be cancelled later in the Heisenberg equation of motion (discussed in Appendix C) so we will ignore this term when presenting the Hamiltonian.

## Appendix B: Geometric term generated by $\hat{\mathcal{D}}(\alpha(t))$

We notice  $\hat{\mathcal{D}}(\alpha(t))$  is a unitary matrix. So it can be generated by the following differential equation

$$\dot{\mathcal{D}}(t) = -i\hat{H}(t)\hat{\mathcal{D}}(t), \quad (\text{B1})$$

where the effective Hamiltonian is

$$\hat{H}(t) = i[\dot{\alpha}(t)\hat{a}^\dagger - \dot{\alpha}^*(t)\hat{a}] + c(t), \quad (\text{B2})$$

and  $c(t)$  is a time-dependent c-number. To prove this, we first show the commutator

$$[\hat{H}(t_1), \hat{H}(t_2)] = -[\dot{\alpha}(t_1)\hat{a}^\dagger - \dot{\alpha}^*(t_1)\hat{a}, \dot{\alpha}(t_2)\hat{a}^\dagger - \dot{\alpha}^*(t_2)\hat{a}] = -\dot{\alpha}(t_1)\dot{\alpha}^*(t_2) + \dot{\alpha}^*(t_1)\dot{\alpha}(t_2) \quad (\text{B3})$$

is also a c-number. Then we use the Magnus expansion to calculate the time-evolution operator

$$T_+ \exp\left\{-i \int_0^t \hat{H}(\tau) d\tau\right\} = \exp\left\{-i \int_0^t \hat{H}(\tau) d\tau - \frac{1}{2} \int_0^t \int_0^{t_1} [\hat{H}(t_1), \hat{H}(t_2)] dt_1 dt_2\right\} \quad (\text{B4a})$$

$$= \exp\{\alpha(t)\hat{a}^\dagger - \alpha^*(t)\hat{a} - \alpha(0)\hat{a}^\dagger + \alpha^*(0)\hat{a} - f(t)\}. \quad (\text{B4b})$$

If we choose

$$ic(t) = \frac{1}{2}[\dot{\alpha}(t)\alpha^*(t) - \dot{\alpha}^*(t)\alpha(t)] , \quad (\text{B5})$$

then  $f(t) = 0$  in Eq. (B4b). We end up with

$$T_+ \exp\left\{-i \int_0^t \hat{H}(\tau) d\tau\right\} \hat{\mathcal{D}}(0) = \exp\{\alpha(t)\hat{a}^\dagger - \alpha^*(t)\hat{a}\} \equiv \hat{\mathcal{D}}(t) , \quad (\text{B6})$$

which gives Eq. (B1) when taking derivative on both sides. Finally, The geometric term  $-i\hat{\mathcal{D}}^\dagger \dot{\hat{\mathcal{D}}}$  is

$$-i\hat{\mathcal{D}}^\dagger \dot{\hat{\mathcal{D}}} = -\hat{\mathcal{D}}^\dagger \hat{H}(t)\hat{\mathcal{D}} = i[\dot{\alpha}^*(t)\hat{a} - \dot{\alpha}(t)\hat{a}^\dagger] , \quad (\text{B7})$$

where we ignored the term that is proportional to identity.

### Appendix C: Input-output formalism in the interaction picture

In this section, we derive the Heisenberg equation of motion in the displacement frame according to the input-output formalism of quantum optics [27]. We assume each resonator mode in our configuration couples to an infinite number of bosonic bath via the interaction Hamiltonian

$$\hat{H}_{\text{int}} = i \sum_{i,k} \gamma_{i,k} \left( \hat{b}_{i,k} \hat{a}_i^\dagger - \hat{a}_i \hat{b}_{i,k}^\dagger \right) , \quad i \in \{\text{e, o, m}\} , \quad (\text{C1})$$

and the pure bath Hamiltonian

$$\hat{H}_{\text{B}} = \sum_{i,k} \omega_{i,k} \hat{b}_{i,k}^\dagger \hat{b}_{i,k} . \quad (\text{C2})$$

In the interaction picture of the laser frequencies, the interaction Hamiltonian becomes

$$\hat{H}_{\text{int}} = i \sum_{i,k} \gamma_{i,k} \left( \hat{a}_i \hat{b}_{i,k}^\dagger e^{-i\omega_{li}t} - \hat{b}_{i,k} e^{i\omega_{li}t} \hat{a}_i^\dagger \right) . \quad (\text{C3})$$

Next, we rotate the interaction Hamiltonian Eq. (C3) with respect to the displacement operator  $\hat{\mathcal{D}} = \otimes_i \hat{\mathcal{D}}_i(\alpha_i(t))$ . The overall effect will be to replace the annihilation and creation operators with

$$\hat{a}_i \rightarrow \hat{a}_i + \alpha_i(t) , \quad \hat{a}_i^\dagger \rightarrow \hat{a}_i^\dagger + \alpha_i^*(t) . \quad (\text{C4})$$

Then we can follow the procedure in [27] to derive the equation of motion. We start by writing down the equation of motion for  $\hat{a}_i(t)$  and  $\hat{b}_{i,k}(t)$

$$\dot{\hat{a}}_i = i \left[ \hat{H}_{\text{lin}}, \hat{a}_i(t) \right] - \sum_k \gamma_{i,k} e^{i\omega_{li}t} \hat{b}_{i,k}(t) \quad (\text{C5a})$$

$$\dot{\hat{b}}_{i,k} = -i\omega_k \hat{b}_{i,k}(t) + \gamma_{i,k} e^{-i\omega_{li}t} (\hat{a}_i(t) + \alpha_i(t)) , \quad (\text{C5b})$$

where we omitted the time-dependence of all the operators on the LHS. The formal solution to Eq. (C5b) is

$$\hat{b}_{i,k} = e^{-i\omega_k(t-t_0)} \hat{b}_{i,k}(0) + \gamma_{i,k} \int_{t_0}^t e^{-i\omega_k(t-\tau)} (\hat{a}_i(\tau) + \alpha_i(\tau)) d\tau , \quad (\text{C6})$$

where  $\hat{b}_{i,k}(0) = \hat{b}_{i,k}$ . Plugging Eq. (C6) into Eq. (C5a), we have

$$\dot{\hat{a}}_i = i[H_{\text{lin}}, \hat{a}_i(t)] - \sum_k \gamma_{i,k} e^{i\omega_{li}t} e^{-i\omega_k(t-t_0)} \hat{b}_{i,k} - \sum_k \gamma_{i,k}^2 e^{i\omega_{li}t} \int_{t_0}^t e^{-i\omega_k(t-\tau)} (\hat{a}_i(\tau) + \alpha_i(\tau)) e^{-i\omega_{li}\tau} d\tau . \quad (\text{C7})$$

Then we make the Markov approximation and replace the summation with an integral  $\sum_k \gamma_{i,k}^2 \rightarrow \gamma_i^2 \int d\omega$ , the last term in Eq. (C7) becomes

$$\gamma_i^2 e^{i\omega_{li}t} \int_{t_0}^t \int_{-\infty}^{\infty} e^{-i\omega(t-\tau)} d\omega (\hat{a}_i^\dagger(\tau) + \alpha_i(\tau)) e^{-i\omega_{li}\tau} d\tau = 2\pi\gamma_i^2 e^{i\omega_{li}t} \int_{t_0}^t \delta(t-\tau) (\hat{a}_i^\dagger(\tau) + \alpha_i(\tau)) e^{-i\omega_{li}\tau} d\tau \quad (\text{C8a})$$

$$= \frac{\kappa_i}{2} (\hat{a}_i(t) + \alpha(t)), \quad (\text{C8b})$$

where  $\kappa_i = 2\pi\gamma_i^2$ . We notice that  $\frac{\kappa_i}{2}\alpha(t)$  in line (C8b) would cancel the terms in line (A7b), so we will ignore those terms in later discussions. Using the standard treatment of input-output formalism, Eq. (C7) becomes

$$\dot{\hat{a}}_i = i [\hat{H}_{\text{lin}}, \hat{a}_i(t)] - \frac{\kappa_i}{2} \hat{a}_i(t) + \sqrt{\kappa_i} \hat{a}_{i,\text{in}}(t), \quad (\text{C9})$$

where

$$\hat{a}_{i,\text{in}}(t) = -\frac{1}{\sqrt{2\pi}} \sum_k e^{-i(\omega_k - \omega_{li})t + i\omega_k t_0} \hat{b}_{i,k}. \quad (\text{C10})$$

For simplicity, we will set  $t_0 = 0$  henceforth. The new expression for the input field is

$$\hat{a}_{i,\text{in}}(t) = -\frac{1}{\sqrt{2\pi}} \sum_k e^{-i(\omega_k - \omega_{li})t} \hat{b}_{i,k}. \quad (\text{C11})$$

Eq. (C11) can be written in the continuous limit

$$\hat{a}_{i,\text{in}}(t) = -\frac{1}{\sqrt{2\pi}} \int_{-\infty}^{\infty} e^{-i\omega t} \hat{b}_i(\omega) d\omega \quad (\text{C12})$$

by shifting the central frequency  $\omega = \omega_k - \omega_{li}$  and replace the summation with integral. Its Fourier transform is given by

$$\hat{a}_{i,\text{in}}(\omega) = \int_{-\infty}^{\infty} \hat{a}_{i,\text{in}}(t) e^{i\omega t} dt = -\sqrt{2\pi} \hat{b}_i(\omega). \quad (\text{C13})$$

In the continuous limit, the commutation relation becomes

$$[\hat{a}_{i,\text{in}}(t), \hat{a}_{i,\text{in}}^\dagger(t')] = \delta(t - t'), \quad [\hat{b}_i(\omega), \hat{b}_i^\dagger(\omega')] = \delta(\omega - \omega'). \quad (\text{C14})$$

We emphasize that the Fourier transform and the Hermitian conjugation do not commute, i.e.,  $\mathcal{F}[\hat{a}_{i,\text{in}}(t)]^\dagger \neq \mathcal{F}[\hat{a}_{i,\text{in}}^\dagger(t)]$ . In this paper, we use the notation

$$\hat{a}_{i,\text{in}}^\dagger(\omega) \equiv \mathcal{F}[\hat{a}_{i,\text{in}}^\dagger(t)](\omega), \quad \hat{a}_{i,\text{in}}(\omega)^\dagger \equiv \{\mathcal{F}[\hat{a}_{i,\text{in}}(t)](\omega)\}^\dagger, \quad (\text{C15})$$

and they satisfy  $\hat{a}_{i,\text{in}}(\omega)^\dagger = \hat{a}_{i,\text{in}}^\dagger(-\omega)$ . As a result, the commutation relation is re-normalized by an additional  $2\pi$  factor

$$[\hat{a}_{i,\text{in}}(\omega), \hat{a}_{i,\text{in}}(\omega')^\dagger] = 2\pi\delta(\omega - \omega'), \quad (\text{C16})$$

for operator  $\hat{a}_{i,\text{in}}(\omega)$ .

In addition, we note that the input modes can be split into multiple parts depending on how we group the bath modes

$$\dot{\hat{a}} = i [\hat{H}_{\text{S}}, \hat{a}] - \frac{\kappa}{2} \hat{a} + \sum_k \sqrt{\kappa_k} \hat{a}_{k,\text{in}}, \quad (\text{C17})$$

where  $\kappa = \sum_k \kappa_k$ . The same procedure can be applied to derive the equations with output modes

$$\dot{\hat{a}} = i [\hat{H}_{\text{S}}, \hat{a}] + \frac{\kappa}{2} \hat{a} - \sum_k \sqrt{\kappa_k} \hat{a}_{k,\text{out}}. \quad (\text{C18})$$

The fundamental relation between the input field and out field can be obtained by combining Eq. (C17) and (C18)

$$\sum_k [\sqrt{\kappa_k} \hat{a}_{\text{out}}(t) + \sqrt{\kappa_k} \hat{a}_{\text{in}}(t)] = \kappa \hat{a}(t). \quad (\text{C19})$$

In practice, stronger conditions

$$\sqrt{\kappa_k} \hat{a}_{\text{out}}(t) + \sqrt{\kappa_k} \hat{a}_{\text{in}}(t) = \kappa_k \hat{a}(t), \quad \forall k \quad (\text{C20})$$

are enforced.

## Appendix D: Equation of motion

Given the equation of motion with input operator Eq. (C17), we can write down the equation of motion subject to the transducer Hamiltonian Eq. (A7). First we denote the state vector as

$$\mathbf{a}(t) = [\hat{a}_o(t), \hat{a}_e(t), \hat{a}_o^\dagger(t), \hat{a}_e^\dagger(t), \hat{a}_m(t), \hat{a}_m^\dagger(t)]^T. \quad (D1)$$

Then we consider the simplest model where each resonator is connected to one input and output mode. In this case, the input and output vectors can be written as

$$\mathbf{a}_{in}(t) = [\hat{a}_{o,in}(t), \hat{a}_{e,in}(t), \hat{a}_{o,in}^\dagger(t), \hat{a}_{e,in}^\dagger(t), \hat{a}_{m,in}(t), \hat{a}_{m,in}^\dagger(t)]^T \quad (D2a)$$

$$\mathbf{a}_{out}(t) = [\hat{a}_{o,out}(t), \hat{a}_{e,out}(t), \hat{a}_{o,out}^\dagger(t), \hat{a}_{e,in}^\dagger(t), \hat{a}_{m,in}(t), \hat{a}_{m,out}^\dagger(t)]^T. \quad (D2b)$$

Explicitly writing down the equation of motion (Eq. (C17)) for each operator in the state vector (Eq. (D1)), we have

$$\begin{aligned} \dot{a}_m &= i[H_{lin}, a_m] = -(i\omega_m + \frac{\kappa_m}{2})a_m - iG_o^*(t)a_o - iG_o(t)a_o^\dagger - iG_e^*(t)a_e - iG_e(t)a_e^\dagger \\ &\quad - i|G_o(t)|^2 - i|G_e(t)|^2 + \sqrt{\kappa_{ex,m}}a_{m,in} \end{aligned} \quad (D3a)$$

$$\begin{aligned} \dot{a}_m^\dagger &= i[H_{lin}, a_m^\dagger] = (i\omega_m - \frac{\kappa_m}{2})a_m^\dagger + iG_o^*(t)a_o + iG_o(t)a_o^\dagger + iG_e^*(t)a_e + iG_e(t)a_e^\dagger \\ &\quad + i|G_o(t)|^2 + i|G_e(t)|^2 + \sqrt{\kappa_{ex,m}}a_{m,in}^\dagger \end{aligned} \quad (D3b)$$

$$\dot{a}_o = i[H_{lin}, a_o] = -i\Delta_o a_o - \frac{\kappa_o}{2}a_o - iG_o(t)(a_m + a_m^\dagger) + \sqrt{\kappa_{ex,o}}a_{o,in} \quad (D3c)$$

$$\dot{a}_o^\dagger = i[H_{lin}, a_o^\dagger] = i\Delta_o a_o^\dagger - \frac{\kappa_o}{2}a_o^\dagger + iG_o^*(t)(a_m + a_m^\dagger) + \sqrt{\kappa_{ex,o}}a_{o,in}^\dagger \quad (D3d)$$

$$\dot{a}_e = i[H_{lin}, a_e] = -i\Delta_e a_e - \frac{\kappa_e}{2}a_e - iG_e(t)(a_m + a_m^\dagger) + \sqrt{\kappa_{ex,e}}a_{e,in} \quad (D3e)$$

$$\dot{a}_e^\dagger = i[H_{lin}, a_e^\dagger] = i\Delta_e a_e^\dagger - \frac{\kappa_e}{2}a_e^\dagger + iG_e^*(t)(a_m + a_m^\dagger) + \sqrt{\kappa_{ex,e}}a_{e,in}^\dagger, \quad (D3f)$$

where  $\kappa_i$  is the total energy decaying rate of the corresponding resonator mode and  $\kappa_{ex,i}$  is the coupling strength between the resonator mode and the input/output field. In the above equations, we omitted the hat symbol for the operators. Eqs. (D3) can be written into a compact matrix form

$$\dot{\mathbf{a}}(t) = \mathbf{A}(t)\mathbf{a}(t) + \mathbf{B}\mathbf{a}_{in}(t) + \mathbf{v}(t), \quad (D4)$$

where

$$\mathbf{A}(t) = \begin{pmatrix} -i\Delta_o - \frac{\kappa_o}{2} & 0 & 0 & 0 & -iG_o(t) & -iG_o(t) \\ 0 & -i\Delta_e - \frac{\kappa_e}{2} & 0 & 0 & -iG_e(t) & -iG_e(t) \\ 0 & 0 & i\Delta_o - \frac{\kappa_o}{2} & 0 & iG_o^*(t) & iG_o^*(t) \\ 0 & 0 & 0 & i\Delta_e - \frac{\kappa_e}{2} & iG_e^*(t) & iG_e^*(t) \\ -iG_o^*(t) & -iG_e^*(t) & -iG_o(t) & -iG_e(t) & -i\omega_m - \frac{\kappa_m}{2} & 0 \\ iG_o^*(t) & iG_e^*(t) & iG_o(t) & iG_e(t) & 0 & i\omega_m - \frac{\kappa_m}{2} \end{pmatrix} \quad (D5a)$$

$$\mathbf{B} = \text{diag}(\sqrt{\kappa_{o,ex}}, \sqrt{\kappa_{e,ex}}, \sqrt{\kappa_{o,ex}}, \sqrt{\kappa_{e,ex}}, \sqrt{\kappa_{m,ex}}, \sqrt{\kappa_{m,ex}}) \quad (D5b)$$

$$\mathbf{v}(t) = [0, 0, 0, 0, -ig_o|\alpha_o(t)|^2 - ig_o|\alpha_e(t)|^2, ig_o|\alpha_o(t)|^2 + ig_e|\alpha_e(t)|^2]^T. \quad (D5c)$$

In addition the input-output formalism ( Eq. (C20)) also has a matrix form, given by

$$\mathbf{a}_{out}(t) + \mathbf{a}_{in}(t) = \mathbf{B}\mathbf{a}(t). \quad (D6)$$

We emphasize that, in Eqs. (D3), we omitted some of the input operators for simplicity. This is permissible because if we average over both sides of Eq. (D4), those inputs connected to either the vacuum or thermal state become 0. However, when we need to calculate the second order moments, those input operators cannot be omitted. In this case, Eq. (D6) becomes

$$\mathbf{a}_{out}(t) + \mathbf{C}\mathbf{a}_{in}(t) = \mathbf{K}\mathbf{a}(t), \quad (D7)$$

where matrices  $\mathbf{B}$ ,  $\mathbf{C}$  and  $\mathbf{K}$  are chosen according to Eq. (C20).

## Appendix E: Frequency domain analysis

### 1. Constant driving

If the control signal  $\Omega_i(t)$  in Eq. (A4) is time-independent, the steady state solution of  $\alpha_i(t)$  is also a constant

$$\alpha_i(t) = \frac{2\Omega_i}{i\kappa_i - 2\Delta_i}. \quad (\text{E1})$$

Then it is most convenient to solve the equation of motion Eq. (D4) in the frequency domain assuming  $\mathbf{A}(t)$  takes its steady state value. Because, in the long time limit,  $\mathbf{v}(t)$  becomes a constant vector, it can be merged into the input vector as a DC component. In general, we are not interested in the transfer function at 0 frequency, so we can solve equation  $\dot{\mathbf{a}}(t) = \mathbf{A}\mathbf{a}(t) + \mathbf{B}\mathbf{a}_{\text{in}}(t)$  instead. In the frequency domain, the equation is

$$-i\omega\mathbf{a}(\omega) = \mathbf{A}\mathbf{a}(\omega) + \mathbf{B}\mathbf{a}_{\text{in}}(\omega), \quad (\text{E2})$$

where we use the convention of  $\int f(t)e^{i\omega t} dt$  for the Fourier transform. Combing Eq. (D6) and (E2), we obtain the transfer function  $T(\omega)$

$$\mathbf{a}_{\text{out}} = \left[ \mathbf{B}(-i\omega\mathbf{I} - \mathbf{A})^{-1}\mathbf{B} - \mathbf{I} \right] \mathbf{a}_{\text{in}} \equiv \mathbf{T}(\omega)\mathbf{a}_{\text{in}}. \quad (\text{E3})$$

In an ideal experimental setup, we would have  $\Delta_o = \Delta_e = \omega_m$ . In this limit, the transmission coefficient at  $\omega_m$  is

$$\begin{aligned} \mathbf{T}_{o,e}(\omega_m) &\equiv \frac{\hat{a}_{o,\text{out}}(\omega_m)}{\hat{a}_{e,\text{in}}(\omega_m)} \\ &= \frac{32\omega_m\sqrt{\kappa_{o,\text{ex}}}\sqrt{\kappa_{e,\text{ex}}}(\kappa_e - 4i\omega_m)(\kappa_o - 4i\omega_m)G_e^*G_o}{64\omega_m^2\kappa_o(i\kappa_o + 4\omega_m)|G_e|^2 + \kappa_e(i\kappa_e + 4\omega_m)\left(-\kappa_m\kappa_o(\kappa_m - 4i\omega_m)(\kappa_o - 4i\omega_m) + 64\omega_m^2|G_o|^2\right)}, \end{aligned} \quad (\text{E4})$$

where  $G_o$  and  $G_e$  all take their steady state values

$$G_i = \frac{2g_i\Omega_i}{i\kappa_i - 2\omega_m}. \quad (\text{E5})$$

If the cavities are ideal and symmetric, i.e.,  $\kappa_{e,\text{ex}} = \kappa_{o,\text{ex}} = \kappa_e = \kappa_o = \kappa$ ,  $g_e = g_o$ , and  $\Omega_o = \Omega_e$ , the transmission coefficient and transduction efficiency becomes

$$\mathbf{T}_{o,e}(\omega_m) = -1 - \frac{i\kappa}{4\omega_m}, \quad \eta(\omega_m) \equiv |\mathbf{T}_{o,e}(\omega_m)| = \sqrt{1 + \frac{\kappa^2}{16\omega_m^2}}. \quad (\text{E6})$$

Other elements of the transfer matrix connecting  $\hat{a}_{o,\text{out}}(\omega_m)$  to the input operators are

$$\mathbf{T}_{o,o}(\omega_m) = -\frac{i\kappa}{4\omega_m}, \quad \mathbf{T}_{o,o^\dagger}(\omega_m) = \mathbf{T}_{o,e^\dagger}(\omega_m) = -\frac{i\kappa G}{4\omega_m G^*}. \quad (\text{E7})$$

From Eq. (E6) and (E7), we can see the noiseless transduction can only be achieved in the resolved sideband limit  $4\omega_m \gg \kappa$ . The same quantities in the case of constant control is

### 2. Oscillating drive

If the control signal in Eq. (A4) is an oscillating function  $\Omega_i(t) = \Omega_i e^{-2i\omega_m t}$ , the steady state solution of  $\alpha_i(t)$  is also a single frequency oscillating function

$$\alpha_i(t) = \frac{2\Omega_i}{4\omega_m - 2\Delta_i + i\kappa_i} e^{-2i\omega_m t}. \quad (\text{E8})$$

As a result, the steady state  $\mathbf{A}(t)$  matrix (Eq. (D5a)) can be written as a Fourier series

$$\mathbf{A}(t) = \mathbf{A}_d + \mathbf{A}_- e^{-2i\omega_m t} + \mathbf{A}_+ e^{2i\omega_m t}, \quad (\text{E9})$$

where

$$\mathbf{A}_d = \begin{pmatrix} -i\Delta_o - \frac{\kappa_o}{2} & 0 & 0 & 0 & 0 & 0 \\ 0 & -i\Delta_e - \frac{\kappa_e}{2} & 0 & 0 & 0 & 0 \\ 0 & 0 & i\Delta_o - \frac{\kappa_o}{2} & 0 & 0 & 0 \\ 0 & 0 & 0 & i\Delta_e - \frac{\kappa_e}{2} & 0 & 0 \\ 0 & 0 & 0 & 0 & -i\omega_m - \frac{\kappa_m}{2} & 0 \\ 0 & 0 & 0 & 0 & 0 & i\omega_m - \frac{\kappa_m}{2} \end{pmatrix} \quad (E10a)$$

$$\mathbf{A}_- = \begin{pmatrix} 0 & 0 & 0 & -iG_o & -iG_o \\ 0 & 0 & 0 & -iG_e & -iG_e \\ 0 & 0 & 0 & 0 & 0 \\ 0 & 0 & 0 & 0 & 0 \\ 0 & 0 & -iG_o & -iG_e & 0 \\ 0 & 0 & iG_o & iG_e & 0 \end{pmatrix} \quad (E10b)$$

$$\mathbf{A}_+ = \begin{pmatrix} 0 & 0 & 0 & 0 & 0 & 0 \\ 0 & 0 & 0 & 0 & 0 & 0 \\ 0 & 0 & 0 & iG_o^* & iG_o^* & 0 \\ 0 & 0 & 0 & iG_e^* & iG_e^* & 0 \\ -iG_o^* & -iG_e^* & 0 & 0 & 0 & 0 \\ iG_o^* & iG_e^* & 0 & 0 & 0 & 0 \end{pmatrix}, \quad (E10c)$$

(E10d)

and  $G_o, G_e$  take their corresponding steady state amplitude

$$G_i = \frac{2g_i\Omega_i}{4\omega_m - 2\Delta_i + i\kappa_i}. \quad (E11)$$

The frequency domain equation of motion can then be written as

$$-i\omega\mathbf{a}(\omega) = \mathbf{A}_d\mathbf{a}(\omega) + \mathbf{A}_-\mathbf{a}(\omega - 2\omega_m) + \mathbf{A}_+\mathbf{a}(\omega + 2\omega_m) + \mathbf{B}\mathbf{a}_{in}(\omega), \quad (E12)$$

where again we ignore the  $\mathbf{v}(t)$  term. To obtain a solvable system, we plug frequencies  $\omega + 2k\omega_m$  into Eq. (E12) and assume  $\mathbf{a}_{in}(\omega)$  is zero at all the sidebands

$$\vdots$$

$$-i(\omega - 2N\omega_m)\mathbf{a}(\omega - 2N\omega_m) = \mathbf{A}_d\mathbf{a}(\omega - 2N\omega_m) + \mathbf{A}_-\mathbf{a}(\omega - 2(N+1)\omega_m) + \mathbf{A}_+\mathbf{a}(\omega - 2(N-1)\omega_m) \quad (E13a)$$

$$\vdots$$

$$-i\omega\mathbf{a}(\omega) = \mathbf{A}_d\mathbf{a}(\omega) + \mathbf{A}_-\mathbf{a}(\omega - 2\omega_m) + \mathbf{A}_+\mathbf{a}(\omega + 2\omega_m) + \mathbf{B}\mathbf{a}_{in}(\omega) \quad (E13b)$$

$$\vdots$$

$$-i(\omega + 2N\omega_m)\mathbf{a}(\omega + 2N\omega_m) = \mathbf{A}_d\mathbf{a}(\omega + 2N\omega_m) + \mathbf{A}_-\mathbf{a}(\omega + 2(N-1)\omega_m) + \mathbf{A}_+\mathbf{a}(\omega + 2(N+1)\omega_m) \quad (E13c)$$

$\vdots$

Then we truncate Eq. (E13) by assuming  $\mathbf{a}(\omega + 2k\omega_m) = 0$  for all  $k < -N$  and  $k > N$ . The resulting equations can be solved iteratively. For example, starting from the boundary equation (E13a), we can solve for  $\mathbf{a}(\omega - 2N\omega_m)$  in terms of  $\mathbf{a}(\omega - 2(N-1)\omega_m)$ , resulting in

$$\mathbf{a}(\omega - 2N\omega_m) = \mathbf{X}_-^{[N]}\mathbf{A}_+\mathbf{a}(\omega - 2(N-1)\omega_m), \quad (E14)$$

where  $\mathbf{X}_-^{[N]} = [-i(\omega - 2N\omega_m)\mathbf{I} - \mathbf{A}_d]^{-1}$ . The solution can be plugged into the equation of motion at frequency  $\omega - 2(N-1)\omega_m$  to obtain

$$\mathbf{a}(\omega - 2(N-1)\omega_m) = \mathbf{X}_-^{[N-1]}\mathbf{A}_+\mathbf{a}(\omega - 2(N-2)\omega_m), \quad (E15)$$

where

$$\mathbf{X}_-^{[N-1]} = \left[ -i(\omega - 2(N-1)\omega_m)\mathbf{I} - \mathbf{A}_d - \mathbf{E}_-^{[N]} \right]^{-1} \quad (E16a)$$

$$\mathbf{E}_-^{[N]} = \mathbf{A}_-[-i(\omega - 2N\omega_m)\mathbf{I} - \mathbf{A}_d]^{-1}\mathbf{A}_+. \quad (E16b)$$

By applying the above procedure iteratively, we end up with an recursive relation

$$\mathbf{a}(\omega - 2k\omega_m) = \mathbf{X}_-^{[k]} \mathbf{A}_+ \mathbf{a}(\omega - 2(k-1)\omega_m), \quad (\text{E17})$$

where

$$\Xi_-^{[k]} = \mathbf{A}_- \mathbf{X}_-^{[k]} \mathbf{A}_+, \quad \mathbf{X}_-^{[k]} = \left[ -i(\omega - 2k\omega_m) \mathbf{I} - \mathbf{A}_d - \Xi_-^{[k+1]} \right]^{-1}, \quad (\text{E18})$$

Setting  $k = 1$ , we end up with  $\mathbf{a}(\omega - 2\omega_m) = \mathbf{X}_-^{[1]} \mathbf{A}_+ \mathbf{a}(\omega)$ . A similar expression  $\mathbf{a}(\omega + 2\omega_m) = \mathbf{X}_+^{[1]} \mathbf{A}_- \mathbf{a}(\omega)$  can be obtained by starting from the other boundary equation (E13c) and using

$$\Xi_+^{[k]} = \mathbf{A}_+ \mathbf{X}_+^{[k]} \mathbf{A}_-, \quad \mathbf{X}_+^{[k]} = \left[ -i(\omega + 2k\omega_m) \mathbf{I} - \mathbf{A}_d - \Xi_+^{[k+1]} \right]^{-1}. \quad (\text{E19})$$

Denoting  $\Xi_\pm^{[1]} \equiv \Xi_\pm$ , the central band Eq. (E13b) can then be rewritten as

$$-i\omega \mathbf{a}(\omega) = \{ \mathbf{A}_d + \Xi_-(\omega) + \Xi_+(\omega) \} \mathbf{a}(\omega) + \mathbf{B} \mathbf{a}_{\text{in}}(\omega), \quad (\text{E20})$$

from which a transfer function can be obtained

$$\mathbf{a}_{\text{out}}(\omega) = \left[ \mathbf{B} (-i\omega \mathbf{I} - \mathbf{A}_d - \Xi_- - \Xi_+)^{-1} \mathbf{B} - \mathbf{I} \right] \mathbf{a}_{\text{in}}(\omega) \equiv \mathbf{T}(\omega) \mathbf{a}_{\text{in}}(\omega). \quad (\text{E21})$$

For simplicity, we define the shorthand notation  $\mathbf{X} = (-i\omega \mathbf{I} - \mathbf{A}_d - \Xi_- - \Xi_+)^{-1}$ . Then the transfer matrix can be written as  $\mathbf{T}(\omega) = \mathbf{B} \mathbf{X} \mathbf{B} - \mathbf{I}$ .

The transfer matrix from inputs at sideband frequencies  $\mathbf{a}_{\text{in}}(\omega + 2k\omega_m)$  can also be iteratively calculated using the same procedure described above

$$\mathbf{a}_{\text{out}}(\omega) = \mathbf{T}(\omega) \mathbf{a}_{\text{in}}(\omega) + \sum_{k=1}^N \left[ \mathbf{T}_+^{[k]}(\omega) \mathbf{a}_{\text{in}}(\omega + 2k\omega_m) + \mathbf{T}_-^{[k]}(\omega) \mathbf{a}_{\text{in}}(\omega - 2k\omega_m) \right], \quad (\text{E22})$$

where

$$\mathbf{T}_\pm^{[k]} = \mathbf{B} \mathbf{X} \prod_{i=1}^k \left( \mathbf{A}_\pm \mathbf{X}_\pm^{[i]} \right) \mathbf{B}. \quad (\text{E23})$$

We will prove in Appendix G that  $\mathbf{T}_\pm^{[k]} = 0$  for  $k > 2$ .

It is the result of the Markov approximation that the input at the sideband frequencies couples to the system through the same coupling matrix  $\mathbf{B}$ . In principle,  $\mathbf{B}$  has an implicit frequency dependence and we can define a shorthand notation  $\mathbf{B}_{\pm k} = \mathbf{B}(\omega \pm 2k\omega_m)$  for the couplings to different sidebands. For a system with generic inputs (Eq. (D7)), the most general forms of the transfer functions are

$$\mathbf{T}(\omega) = \mathbf{K} \mathbf{X} \mathbf{B} - \mathbf{C}, \quad \mathbf{T}_\pm^{[k]} = \mathbf{K} \mathbf{X} \prod_{i=1}^k \left( \mathbf{A}_\pm \mathbf{X}_\pm^{[i]} \right) \mathbf{B}_{\pm k}. \quad (\text{E24})$$

Again, in the limit of  $\Delta_o = \Delta_e = \omega_m$ , the transfer function of  $N = 1$  is given by

$$\mathbf{T}_{o,e}(\omega_m) = \frac{32i\omega_m \sqrt{\kappa_{o,\text{ex}}} \sqrt{\kappa_{e,\text{ex}}} G_e^* G_o}{-16i\omega_m \kappa_o |G_e|^2 + \kappa_e \left( \kappa_m \kappa_o (\kappa_m + 4i\omega_m) - 16i\omega_m |G_o|^2 \right)}. \quad (\text{E25})$$

If the cavities are symmetric, i.e.,  $\kappa_{e,\text{ex}} = \kappa_{o,\text{ex}} = \kappa_e = \kappa_o = \kappa$ ,  $g_e = g_o$ , and  $\Omega_o = \Omega_e$ , the transmission coefficient and transduction efficiency become

$$\mathbf{T}_{o,e}(\omega_m) = -1, \quad \eta(\omega_m) \equiv |\mathbf{T}_{o,e}(\omega_m)| = 1. \quad (\text{E26})$$

Eq. (E26) corresponds to the perfect transduction. The expressions for other quantities can be obtained using [31].

## Appendix F: Added noise

In addition to the transduction efficiency, the added noise is another important metric for the bosonic transducer. In the configuration considered in this paper, the total noise is defined as [23, 30]

$$2\pi\eta^2(\omega)S_t(\omega)\delta(\omega - \omega') = \frac{1}{2} \left\langle \left\{ \hat{a}_{o,out}(\omega')^\dagger, \hat{a}_{o,out}(\omega) \right\} \right\rangle - \left\langle \hat{a}_{o,out}(\omega) \right\rangle \left\langle \hat{a}_{o,out}(\omega')^\dagger \right\rangle, \quad (\text{F1})$$

where we explicitly write out the average operator  $\langle \cdot \rangle$  because the first term corresponds to the second order momentum. The  $2\pi$  comes from the normalization factor of the input and output modes (Eq. (C16)). Eq. (F1) can be simplified by substituting

$$\hat{a}_{o,out}(\omega) = \mathbf{T}_{o,e}(\omega)\hat{a}_{e,in}(\omega) + \hat{J}(\omega) \equiv \mathbf{T}_{o,e}(\omega)\hat{a}_{e,in}(\omega) + \hat{J}_{\text{ex}}(\omega) + \hat{J}_{\text{im}}(\omega) \quad (\text{F2})$$

where

$$\hat{J}_{\text{ex}}(\omega) = \mathbf{T}_{o,e^\dagger}(\omega)\hat{a}_{e,in}^\dagger(\omega) + \mathbf{T}_{o,o}(\omega)\hat{a}_{o,in}(\omega) + \mathbf{T}_{o,o^\dagger}(\omega)\hat{a}_{o,in}^\dagger(\omega) \quad (\text{F3})$$

and

$$\hat{J}_{\text{im}}(\omega) = \sum_i \left( \mathbf{T}_{o,i}(\omega)\hat{a}_{i,in} + \mathbf{T}_{o,i^\dagger}(\omega)\hat{a}_{i,in}^\dagger \right). \quad (\text{F4})$$

$\hat{J}(\omega) = \hat{J}_{\text{ex}}(\omega) + \hat{J}_{\text{im}}(\omega)$  are unwanted modes being mixed into the output.  $\hat{J}_{\text{ex}}(\omega)$  contains all the input mode operators explicitly defined in the equation of motion (D4) while  $\hat{J}_{\text{im}}$  has all the implicit terms, i.e., the internal loss ports, the sideband couplings (Eq. (E22)). The terms in  $\hat{J}_{\text{im}}$  all satisfy  $\langle \hat{a}_{i,in} \rangle = \langle \hat{a}_{i,in}^\dagger \rangle = 0$ . To avoid any confusion, we emphasize again how we define operators  $\hat{a}(\omega)^\dagger$  and  $\hat{a}^\dagger(\omega)$  in Eq. (C15). We can simplify the RHS of Eq. (F1) as

$$\text{RHS} = \frac{1}{2} \left\langle \left\{ \hat{J}(\omega), \hat{J}(\omega')^\dagger \right\} \right\rangle + \mathbf{T}_{o,e}(\omega)\mathbf{T}_{o,e}^*(\omega') \left[ \left\langle \left\{ \hat{a}_{e,in}(\omega), \hat{a}_{e,in}(\omega')^\dagger \right\} \right\rangle / 2 - \left\langle \hat{a}_{e,in}(\omega) \right\rangle \left\langle \hat{a}_{e,in}(\omega')^\dagger \right\rangle \right] \quad (\text{F5a})$$

$$+ \frac{\mathbf{T}_{o,e}(\omega)\mathbf{T}_{o,e^\dagger}^*(\omega')}{2} \langle \{ \hat{a}_{e,in}(\omega), \hat{a}_{e,in}(-\omega') \} \rangle + \frac{\mathbf{T}_{o^\dagger,e^\dagger}^*(\omega')\mathbf{T}_{o,e^\dagger}(\omega)}{2} \langle \{ \hat{a}_{e,in}^\dagger(\omega), \hat{a}_{e,in}^\dagger(-\omega') \} \rangle \quad (\text{F5b})$$

$$- \mathbf{T}_{o,e}(\omega)\mathbf{T}_{o,e^\dagger}^*(\omega') \langle \hat{a}_{e,in}(\omega) \rangle \langle \hat{a}_{e,in}(-\omega') \rangle - \mathbf{T}_{o^\dagger,e^\dagger}^*(\omega')\mathbf{T}_{o,e^\dagger}(\omega) \langle \hat{a}_{e,in}^\dagger(\omega) \rangle \langle \hat{a}_{e,in}^\dagger(-\omega') \rangle, \quad (\text{F5c})$$

where we assume  $\langle \hat{a}_{o,in}(\omega) \rangle = 0$  and all the inputs are not correlated with each other. Finally, since the average is over a coherent state, lines (F5b) and (F5c) add up to 0. The second term in line (F5a) equals  $\pi\eta^2(\omega)\delta(\omega - \omega')$ , which set a lower bound to  $S_t(\omega) \geq \frac{1}{2}$ , is the quantum limit of the transduction noise. It represents the vacuum fluctuation. Finally, the first term in line (F5a) gives the expression of added noise

$$2\pi\eta^2(\omega)S(\omega)\delta(\omega - \omega') = \frac{1}{2} \left\langle \left\{ \hat{J}(\omega), \hat{J}(\omega')^\dagger \right\} \right\rangle. \quad (\text{F6})$$

The RHS of Eq. (F6) can be explicitly written out as

$$\frac{1}{2} \left\langle \left\{ \hat{J}(\omega), \hat{J}(\omega')^\dagger \right\} \right\rangle = \frac{1}{2} |\mathbf{T}_{o,e^\dagger}(\omega)|^2 \left\langle \left\{ \hat{a}_{e,in}(\omega)^\dagger, \hat{a}_{e,in}(\omega') \right\} \right\rangle \quad (\text{F7a})$$

$$+ \frac{1}{2} |\mathbf{T}_{o,o}(\omega)|^2 \left\langle \left\{ \hat{a}_{o,in}(\omega), \hat{a}_{o,in}(\omega')^\dagger \right\} \right\rangle + \frac{1}{2} |\mathbf{T}_{o,o^\dagger}(\omega)|^2 \left\langle \left\{ \hat{a}_{o,in}(\omega)^\dagger, \hat{a}_{o,in}(\omega') \right\} \right\rangle \quad (\text{F7b})$$

$$+ \frac{1}{2} \sum_i \left\{ |\mathbf{T}_{o,i}(\omega)|^2 \left\langle \left\{ \hat{a}_{o,in}, (\hat{a}_{o,in})^\dagger \right\} \right\rangle + |\mathbf{T}_{o,i^\dagger}(\omega)|^2 \left\langle \left\{ (\hat{a}_{i,in})^\dagger, \hat{a}_{i,in} \right\} \right\rangle \right\}. \quad (\text{F7c})$$

If we assume the input of the electrical cavity is a coherent state with a single photon and all other inputs are the vacuum state, Eq. (F7) can be further simplified. Combining Eq. (F6) and (F7), the added noise becomes

$$\eta^2(\omega)S(\omega) = \frac{3}{2} |\mathbf{T}_{o,e^\dagger}(\omega)|^2 + \frac{1}{2} |\mathbf{T}_{o,o}(\omega)|^2 + \frac{1}{2} |\mathbf{T}_{o,o^\dagger}(\omega)|^2 + \frac{1}{2} \sum_i \left( |\mathbf{T}_{o,i}(\omega)|^2 + |\mathbf{T}_{o,i^\dagger}(\omega)|^2 \right). \quad (\text{F8})$$

By allowing the input at the optical cavity to be a squeezed vacuum state, Eq. (F8) can be relaxed into an inequality [23]

$$\eta^2(\omega)S(\omega) \geq \frac{3}{2} |\mathbf{T}_{o,e^\dagger}(\omega)|^2 + \frac{1}{2} \left| |\mathbf{T}_{o,o}(\omega)|^2 - |\mathbf{T}_{o,o^\dagger}(\omega)|^2 \right| + \frac{1}{2} \sum_i \left| |\mathbf{T}_{o,i}(\omega)|^2 - |\mathbf{T}_{o,i^\dagger}(\omega)|^2 \right| \quad (\text{F9a})$$

$$\geq \frac{3}{2} |\mathbf{T}_{o,e^\dagger}(\omega)|^2 + \frac{1}{2} \left| 1 - |\mathbf{T}_{o,e}(\omega)|^2 + |\mathbf{T}_{o,e^\dagger}(\omega)|^2 \right|, \quad (\text{F9b})$$

From line (F9a) to (F9b) we make use of the inequality

$$\sum_i \left| |\mathbf{T}_{o,i}|^2 - |\mathbf{T}_{o,i^\dagger}|^2 \right| \geq \left| \sum_i |\mathbf{T}_{o,i}|^2 - |\mathbf{T}_{o,i^\dagger}|^2 \right| \quad (\text{F10})$$

and

$$1 = |\mathbf{T}_{o,e}(\omega)|^2 - |\mathbf{T}_{o,e^\dagger}(\omega)|^2 + |\mathbf{T}_{o,o}(\omega)|^2 - |\mathbf{T}_{o,o^\dagger}(\omega)|^2 + \sum_i |\mathbf{T}_{o,i}(\omega)|^2 - |\mathbf{T}_{o,i^\dagger}(\omega)|^2. \quad (\text{F11})$$

Eq. (F11) comes from the preservation of commutation  $[\hat{a}_{o,out}(\omega), \hat{a}_{o,out}(\omega)^\dagger] = 2\pi$ . As a result,  $S(\omega)$  has a lower bound

$$S(\omega) \geq \frac{3}{2} R^2(\omega) + \left| \frac{1 - \eta^2(\omega)}{2\eta^2(\omega)} + \frac{R^2(\omega)}{2} \right|, \quad (\text{F12})$$

where  $R^2(\omega) = |\mathbf{T}_{o,e^\dagger}(\omega)|^2 / \eta^2(\omega)$ . The lower bound can only be achieved by squeezing every input port which has non-zero transmission coefficient to the output.

## Appendix G: Structures of $\mathbf{T}(\omega)$ and $\mathbf{T}_\pm^{[k]}(\omega)$

### 1. Block diagonal structure of $\mathbf{T}(\omega)$

The key observation is that the transfer matrix  $\mathbf{T}(\omega)$  in Eq. (E21) have a direct sum structure  $\bigoplus_i \mathcal{L}_i$ ,  $i \in \{a, c, m\}$  where  $\mathcal{L}_i$ s are linear operators  $\mathcal{L}_i : \mathbf{V}_i \rightarrow \mathbf{V}_i$ .  $\mathbf{V}_i$ s are vector spaces spanned by

$$\mathbf{V}_i = \begin{cases} \text{span}([\hat{a}_{o,in}(\omega), \hat{a}_{e,in}(\omega)]) & i = a \\ \text{span}([\hat{a}_{o,in}^\dagger(\omega), \hat{a}_{e,in}^\dagger(\omega)]) & i = c \\ \text{span}([\hat{a}_{m,in}(\omega), \hat{a}_{m,in}^\dagger(\omega)]) & i = m \end{cases}. \quad (\text{G1})$$

Eq. (G1) means  $\mathbf{T}(\omega)$  has a block diagonal form

$$\mathbf{T} = \begin{pmatrix} \mathbf{T}_a & 0 & 0 \\ 0 & \mathbf{T}_c & 0 \\ 0 & 0 & \mathbf{T}_m \end{pmatrix}, \quad (\text{G2})$$

where  $\mathbf{T}_i$ s are  $2 \times 2$  matrices. To prove this statement, we first note  $\mathbf{T} = \mathbf{B} \mathbf{X} \mathbf{B} - \mathbf{I}$ , where  $\mathbf{B}$ , and  $\mathbf{I}$  are diagonal matrices. So a sufficient condition for Eq. (G2) is  $\mathbf{X}$  being block diagonal. We proceed by writing  $\mathbf{A}_+$  (E10c) and  $\mathbf{A}_-$  (E10b) in the block matrix form

$$\mathbf{A}_- = \begin{pmatrix} 0 & 0 & \mathbf{Q}_{am} \\ 0 & 0 & 0 \\ 0 & \mathbf{Q}_{mc} & 0 \end{pmatrix}, \quad \mathbf{A}_+ = \begin{pmatrix} 0 & 0 & 0 \\ 0 & 0 & \mathbf{Q}_{cm} \\ \mathbf{Q}_{ma} & 0 & 0 \end{pmatrix}. \quad (\text{G3})$$

It is straightforward to show that for any given block diagonal matrix

$$\mathbf{D} = \begin{pmatrix} \mathbf{D}_1 & 0 & 0 \\ 0 & \mathbf{D}_2 & 0 \\ 0 & 0 & \mathbf{D}_3 \end{pmatrix}, \quad (\text{G4})$$

$\mathbf{A}_- \mathbf{D} \mathbf{A}_+$  and  $\mathbf{A}_+ \mathbf{D} \mathbf{A}_-$  are also block diagonal

$$\mathbf{A}_- \mathbf{D} \mathbf{A}_+ = \begin{pmatrix} \mathbf{Q}_{am} \mathbf{D}_3 \mathbf{Q}_{ma} & 0 & 0 \\ 0 & 0 & 0 \\ 0 & 0 & \mathbf{Q}_{cm} \mathbf{D}_2 \mathbf{Q}_{mc} \end{pmatrix}, \quad \mathbf{A}_+ \mathbf{D} \mathbf{A}_- = \begin{pmatrix} 0 & 0 & 0 \\ 0 & \mathbf{Q}_{cm} \mathbf{D}_3 \mathbf{Q}_{mc} & 0 \\ 0 & 0 & \mathbf{Q}_{am} \mathbf{D}_1 \mathbf{Q}_{ma} \end{pmatrix}. \quad (\text{G5})$$

Because the inverse of a block diagonal matrix is still block diagonal, we can deduce  $\mathbf{X}_\pm^{[k]}$  and  $\mathbf{\Xi}_\pm^{[k]}$  are block diagonal from the recursive relation

$$\mathbf{\Xi}_\pm^{[k]} = \mathbf{A}_\pm \mathbf{X}_\pm^{[k]} \mathbf{A}_\mp, \quad \mathbf{X}_\pm^{[k]} = \left[ -i(\omega \pm 2k\omega_m) \mathbf{I} - \mathbf{A}_d - \mathbf{\Xi}_\pm^{[k+1]} \right]^{-1}, \quad \mathbf{X}_\pm^{[N]} = \left[ -i(\omega \pm 2N\omega_m) \mathbf{I} - \mathbf{A}_d \right]^{-1}. \quad (\text{G6})$$

As a result,  $\mathbf{X} = \left( -i\omega \mathbf{I} - \mathbf{A}_d - \mathbf{\Xi}_-^{[1]} - \mathbf{\Xi}_+^{[1]} \right)^{-1}$ , thus  $\mathbf{T}$ , are also block diagonal.

2.  $\mathbf{T}_{\pm}^{[k]}(\omega) = 0$  for  $k > 2$

Based on the above observations, we can also prove  $\mathbf{T}_{\pm}^{[k]} = 0$  for  $k > 2$ . The expression for  $\mathbf{T}_{\pm}^{[k]}$  is given in Eq. (E23) and repeated below for clarity:

$$\mathbf{T}_{\pm}^{[k]} = \mathbf{B} \mathbf{X} \prod_{i=1}^k \left( \mathbf{A}_{\pm} \mathbf{X}_{\pm}^{[i]} \right) \mathbf{B} . \quad (\text{G7})$$

From Sec. G 1, we already knew that  $\mathbf{X}$  and  $\mathbf{X}_{\pm}^{[i]}$  are block-diagonal. Next, we show

$$\prod_{i=1}^k (\mathbf{A}_{\pm} \mathbf{D}_i) = 0 \quad \forall k > 2 , \quad (\text{G8})$$

for any block diagonal matrices  $\mathbf{D}_i = \text{diag}(\mathbf{D}_{i1}, \mathbf{D}_{i2}, \mathbf{D}_{i3})$ . This can be done by writing down the case of  $k = 1, 2$  explicitly

$$\mathbf{A}_{-} \mathbf{D}_1 = \begin{pmatrix} 0 & 0 & \mathbf{Q}_{\text{am}} \mathbf{D}_{13} \\ 0 & 0 & 0 \\ 0 & \mathbf{Q}_{\text{mc}} \mathbf{D}_{12} & 0 \end{pmatrix} , \quad \mathbf{A}_{-} \mathbf{D}_2 \mathbf{A}_{-} \mathbf{D}_1 = \begin{pmatrix} 0 & \mathbf{Q}_{\text{am}} \mathbf{D}_{23} \mathbf{Q}_{\text{mc}} \mathbf{D}_{12} & 0 \\ 0 & 0 & 0 \\ 0 & 0 & 0 \end{pmatrix} . \quad (\text{G9})$$

Then it is straightforward to check  $\prod_{i=1}^3 (\mathbf{A}_{-} \mathbf{D}_i) = 0$ , thus  $\prod_{i=1}^k (\mathbf{A}_{-} \mathbf{D}_i) = 0$ , for  $k > 3$ . The same is also true for  $\prod_{i=1}^k (\mathbf{A}_{+} \mathbf{D}_i)$ , where

$$\mathbf{A}_{+} \mathbf{D}_1 = \begin{pmatrix} 0 & 0 & 0 \\ 0 & 0 & \mathbf{Q}_{\text{cm}} \mathbf{D}_{13} \\ \mathbf{Q}_{\text{ma}} \mathbf{D}_{11} & 0 & 0 \end{pmatrix} , \quad \mathbf{A}_{+} \mathbf{D}_2 \mathbf{A}_{+} \mathbf{D}_1 = \begin{pmatrix} 0 & 0 & 0 \\ \mathbf{Q}_{\text{cm}} \mathbf{D}_{23} \mathbf{Q}_{\text{ma}} \mathbf{D}_{11} & 0 & 0 \\ 0 & 0 & 0 \end{pmatrix} . \quad (\text{G10})$$

Knowing  $\mathbf{X}_{\pm}^{[i]}$  is block diagonal, we prove  $\mathbf{T}_{\pm}^{[k]} = 0$  for  $k > 2$  by combining Eq. (G7) and (G8).

We notice  $\mathbf{T}_{\pm}^{[1]}$  only couples the elements from subspaces  $\mathbf{V}_a$  and  $\mathbf{V}_m$  or  $\mathbf{V}_c$  and  $\mathbf{V}_m$ , while  $\mathbf{T}_{\pm}^{[2]}$  only couples the elements from subspaces  $\mathbf{V}_a$  and  $\mathbf{V}_c$ , by further examining the structure of  $\mathbf{T}_{\pm}^{[1]}$  and  $\mathbf{T}_{\pm}^{[2]}$ . As a result, the only terms being mixed into the output (as appeared in Eq. (F4)) by  $\mathbf{T}_{\pm}^{[1]}$  and  $\mathbf{T}_{\pm}^{[2]}$  are

$$\hat{a}_{o,\text{out}}(\omega) = \cdots + \mathbf{T}_{-}^{[1]}[o, m] \hat{a}_{m,\text{in}}(\omega - 2\omega_m) + \mathbf{T}_{-}^{[1]}[o, m^{\dagger}] \hat{a}_{m,\text{in}}^{\dagger}(\omega - 2\omega_m) + \quad (\text{G11a})$$

$$+ \mathbf{T}_{-}^{[2]}[o, e^{\dagger}] \hat{a}_{e,\text{in}}^{\dagger}(\omega - 4\omega_m) + \mathbf{T}_{-}^{[2]}[o, o^{\dagger}](\omega) \hat{a}_{o,\text{in}}^{\dagger}(\omega - 4\omega_m) \cdots \quad (\text{G11b})$$

where  $\mathbf{T}[a, b]$  is a shorthand notation for the element in  $\mathbf{T}$  which couples component  $a$  and  $b$ .

For the generic case Eq. (E24), similar results can also be proved because  $\mathbf{X}$  and  $\mathbf{X}_{\pm}^{[i]}$  are block diagonal and the matrices  $\mathbf{B}$ ,  $\mathbf{K}$ , and  $\mathbf{C}$  does not couple elements from different subspaces (they are chosen according to Eq. (C20)).

## Appendix H: Numerical values

Table I provides all the numerical values used in the paper. Most of the values are chosen according to this experiment [13]. The coupling strength to the internal loss ports of the EM cavities are calculated by  $\kappa_{i,\text{int}} = \kappa_i - \kappa_{i,\text{ex}}$ . We always assume that the mechanical mode has a single input and output, i.e.,  $\kappa_{m,\text{ex}} = \kappa_m$ .

parameter	value	parameter	value	parameter	value
$\Delta_o/2\pi$	1.11 MHz	$\Delta_e/2\pi$	1.47 MHz	$\omega_m/2\pi$	1.4732 MHz
$\kappa_o/2\pi$	2.1 MHz	$\kappa_e/2\pi$	2.5 MHz	$\kappa_m/2\pi$	11 Hz
$\kappa_{o,\text{ex}}/2\pi$	1.1 MHz	$\kappa_{e,\text{ex}}/2\pi$	2.3 MHz	$\kappa_{m,\text{ex}}/2\pi$	11 Hz
$g_o/2\pi$	6.6 Hz	$g_e/2\pi$	3.8 Hz		

Table I. Numerical values of the parameters used in simulations.